Pakistan Journal of Engineering

Pakistan Journal of Engineering

October 2020, Vol. 1(1)

ISSN NO. 2706-9648
(online)

Pakistan Engineering Council, HQs, Islamabad

Pakistan Journal of Engineering

Pakistan Journal of Engineering

October 2020, Vol. 1(1)

ISSN NO. 2706-9648
(online)

Editor-in-Chief
Pakistan Journal of Engineering
Pakistan Engineering Council, HQ, Islamabad
Email: pecjournal@pec.org.pk

Preface

The Scientific research outcomes and innovative contributions are better disseminated through technical and research journals. No doubt large number of international and national journals are already in place, nevertheless the quality of a good journal rests with its scope, continuity, indexation and citation. PEC being a regulator and promoter of quality higher engineering education, has a role to play for the promotion of quality research and innovation in the country, especially to support the local industry towards indigenous solutions and technology advancement.

With this intent, PEC has taken initiative to publish this research and technical journal covering engineering and technology domain with emphasis on knowledge advancement and creativity through genuine research. It is a technical journal covering the entire engineering regime including technical, management and policy related topics in all disciplines and sub-sectors of engineering, targeting knowledge advancement and innovative solutions.

The standard procedure of online submission, initial scrutiny, reviewers' engagement, manuscript updation and final decision, have been adopted, followed by approvals and publication. There is a complete system of governance including an Advisory Committee and an Editorial Board, comprising eminent professionals (national and internationals), besides reviewers from all sectors and both from industry and academia.

Engr Jawed Salim Qureshi
Patron-in-Chief
Pakistan Journal of Engineering

Editorial Board

Advisory Board

Disclaimer

In accordance with the Review Policy of this Pakistan Journal of Engineering, these Manuscripts have been peer reviewed by our eminent reviewers and experts after quality check, and considerations shared with the authors by Journal Editorial Board. This disclaimer lets that the research work is authors' original creation and is not copied from any other work, except the portions for which the sources are clearly acknowledged therein. The work contains no violation of any existing copyright, other third party rights or any unlawful statements and does not violate any rights of others, and authors agreed to indemnify Pakistan Journal of Engineering against any claims in respect of the above warranties. Since this work is approved after review and being published in the Pakistan Journal of Engineering, the authors' assigned the copyright including, but is not limited to, the right to publish the work, to reproduce it, and to disseminate it, either alone or collectively with other works or in whatever fashion the Journal considers appropriate. The authors reserve all proprietary rights other than copyright such as patent rights and the right to use all or part of this article in future works of their own such as lectures, reviews, personal websites, text books, etc.

ISSN NO. 2706-9648

Contents

ISSN NO. 2706-9648

Pakistan Journal of Engineering

For online access, please visit:
journal.pec.org.pk

CONDITION RATING OF TWO HIGHWAY BRIDGES IN LAHORE AND PROPOSAL FOR BRIDGE PERFORMANCE INDEX (BPI)

M. Azhar Saleem, Salman Bin Rafiq

ARTICLE INFO

Article History:

Accepted 16 Oct 2020

Published on 25 Oct 2020

Keywords

Bridge Health, Condition Rating, Bridge Performance Index, BPI, Assessment, Pakistan.

ABSTRACT

Proactive approach for bridge maintenance is of utmost importance. This paper presents the condition rating of two highway bridges and proposes the concept of bridge performance index (BPI). Thought in the background was to emphasize the need to adopt proactive approach for bridge maintenance. Highway agencies in Pakistan generally adopt reactive approach to address the health issues of bridges, which may leave bridge users in vulnerable situation. Condition rating is an important component of the bridge management system (BMS) and visual inspection is the most widely used method for condition rating. The elements of both bridges were visually inspected and rated, using a scale of 0 to 10. These element level ratings were then integrated to find the span performance indices and the BPI. This index, when refined using larger stock of bridges situated in various parts of the country, may be helpful in optimizing the resource allocation for bridge maintenance. It was observed that nonstructural elements like expansion joints, drainage pipes and bearings catch less attention of maintenance agencies. Poor condition of non-structural elements impacts the health of the structural elements. As a whole, both bridges were in very good condition and only need minor repair. BPI for both bridges was found as 7 on the scale of 10.

1. Introduction

Maintaining bridges is a very challenging task because it involves traffic interruptions, expensive machinery, accessibility problems and special materials in some cases. Bridges need regular maintenance to keep them in service throughout their useful life [12],[30]. This is not only true for a developing country like Pakistan but valid for a developed country like United States. Agencies in

the U.S. are facing great challenge to get rid of the backlog of bridges which need significant maintenance, rehabilitation or replacement [6]. According to 2017 infrastructure report card published by American Society of Civil Engineers, out of total 614,387 bridges in the US, 9.1% also are structurally deficient and 13.6% are functionally obsolete. A hefty estimated amount of $123 billion is needed to rehabilitate bridges in the US [4]. A bridge is classified as structurally deficient if it has considerable damage to its main components and as functionally obsolete if it does not meet the current standards, especially with reference to public safety.

Bridge condition evaluation and rating system in the US mainly started in 1967, when Silver Bridge (a suspension bridge) on Ohio River failed and collapsed in West Virginia resulting in a loss of 46 lives. The incident set a record of twentieth century causalities in a bridge collapse [28]. As a result, National Bridge Inspection Program in the US was launched to develop a bridge rating and inspection system and also to address present and future needs of bridges to optimize their remaining service life (White et al., 1992). The first AASHTO inspection manual was issued in 1970[1]. This manual provides the minimum information requisite for recording, rating and assessing load capacity of bridges [23]. The National Bridge Inspection Standards [13] were established in 1971 to provide instructions and guidelines and to develop consistent and uniform criteria for the various highway agencies. These standards require that each State should maintain a bridge inspection organization. After every two years, bridges are inspected and National Bridge Inventory (NBI) is updated. Historically, the data for NBI has been recorded as per the guidelines of Federal Highway Administration's (FHWA) Recording and Coding Guide [14]. The NBI condition rating used a numeric scale from 0 to 9 for rating purposes, with 9 for excellent and zero for failed condition [14]. Few years ago, FHWA has started using a rating scale of 1 to 4 at the element level. For Bridge Management System (BMS), individual states gather the element condition data. The bridge elements are defined by AASHTO's Guide Manual for Bridge Element Inspection [2].

After the collapse of I-35W Bridge in August 2007, a joint ASCE/ SEI-AASHTO ad-hoc group was formed to review the in-place bridge maintenance and inspection policies. This group recommended that the risk based approach should be adopted to determine the inspection interval for bridges, instead of a pre-defined 2 year cycle. The group also emphasized on the need to develop standard procedures for special inspections involving nondestructive testing and condition monitoring technologies. Bridges which are new or in good condition would be inspected after a period longer than 2 years. For instance, in Europe, longer inspection periods are normal, as much as 6 years in some cases [3]. Washer et al [25] also proposed a framework for risk-based inspection (RBI) of highway bridges. The RBI was implemented on two highway bridges and verified that this approach determined suitable inspection interval for the sample bridges [26].

With few exceptions, currently in Pakistan, reactive approach is adopted when it comes to maintaining bridges. Whenever a problem occurs, highway officials rush to the bridge, fix it and then wait for the next emergency to happen. Pakistan has yet to develop a national bridge inspection manual and acquire proper inspection machinery. There is a need to develop national bridge inventory and thorough investigation of bridges through a well formulated inspection and rehabilitation program. At present, in Pakistan, there is no mandated requirement for periodic inspection of bridges.

The primary objective of current study was to perform condition rating of two highway bridges in the city of Lahore and propose the concept of an index which would represent the condition of concrete highway bridges in Pakistan. The secondary objective was to emphasize on the need to adopt proactive approach for bridge maintenance

and to develop a BMS (bridge management system) in the country. To fulfill these objectives, detailed visual based condition assessment of two bridges situated near Lahore Cantt Railway Station was carried out. In the absence of an integrated BMS, it was very challenging to coordinate with various agencies to collect data/ drawings of these bridges, which were constructed more than forty years ago. Out of total twelve months, first four months were consumed in acquiring necessary documents, permissions from relevant authorities and resources to kick off the project work.

1.1 Condition Rating

The word "condition" has a particular resonance in the bridge engineering fraternity [22]. Condition rating is meant to compare the existing condition of bridge with its condition at the time of construction [11]. The first step in condition assessment of bridges is visual inspection by an experienced inspector. Visual inspection can reveal defects like cracking, scaling, spalling, delamination and corrosion. After visual inspection, the traditional nondestructive testing (NDT) techniques can help in quantifying the extent of damage [10]. Bridge condition rating systems are developed to access the overall condition of bridges. Countries around the world have developed rating systems according to their own circumstances. For instance, Japanese specify deficiency rating which is based on defects like cracking, corrosion and deformation etc. [22], [29]. Five deterioration levels are defined from I to V, with I being potentially hazardous and V being like new [17].

Overall bridge rating is very general and may not be able to highlight the specific problem in the elements, therefore, condition rating is generally carried out at the element level [11]. The FHWA (1995) provides a scale from 0 to 9 for the condition rating of bridge elements. Table 1 provides the details of this scale. Like other systems, this system also does not provide information about the nature and location of potential failure [24]. The assumption in FHWA's system is that bridges remain useful until the rating reaches the value of 3. In New York, all the elements in every span of bridges are inspected at least once in every two years. Weights have been assigned to each element which are used to calculate the overall bridge condition rating (BCR) according to following formula [27].

$$BCR = \frac{\sum(Component\ Rating * Weight)}{\sum Weights} \quad \text{Eq. 1}$$

Table 1. FHWA Element Condition Rating

Rating	Description
N	NOT APPLICABLE
9	EXCELLENT CONDITION
8	VERY GOOD CONDITION - no problems noted.
7	GOOD CONDITION - some minor problems.
6	SATISFACTORY CONDITION - structural elements show some minor deterioration.
5	FAIR CONDITION - all primary structural elements are sound but may have minor section loss, cracking, spalling or scour.
4	POOR CONDITION - advanced section loss, deterioration, spalling or scour.
3	SERIOUS CONDITION - loss of section, deterioration, spalling or scour have seriously affected primary structural components. Local failures are possible. Fatigue cracks in steel or shear cracks in concrete may be present.

2	CRITICAL CONDITION - advanced deterioration of primary structural elements. Fatigue cracks in steel or shear cracks in concrete may be present or scour may have removed substructure support. Unless closely monitored it may be necessary to close the bridge until corrective action is taken.
1	"IMMINENT" FAILURE CONDITION - major deterioration or section loss present in critical structural components or obvious vertical or horizontal movement affecting structure stability. Bridge is closed to traffic but corrective action may put back in light service.
0	FAILED CONDITION - out of service - beyond corrective action.

Elbehairy (2007) suggested that different bridges may have different elements' weights based on the age and function of the element. For example, the deck of a slab bridge must have more weight than the deck of a girder bridge. This variation in the element weights must be included in the BMS. New York State has been rating the bridge condition from 1 to 7, where 1 is for totally deteriorated bridges and 7 is for new bridges [18]. Moscow bridge management system consists of a five-point scale to (Table 2) access bridge condition [8].

Table 2. Moscow Bridge Rating System

Condition	Assessment	Wear	Type of Repair Required
1	Good	Less than 20 %	Cleaning, scheduled maintenance
1.5	Not very good	20 – 40 %	Preventive maintenance
2	Poor	40 – 60 %	Current (local) repair
2.5	Very Poor	60 – 80 %	Major repair
3	Unacceptable	80 – 100 %	Replacement or restoration repair

Ontario Structure Inspection Manual (OSIM 2000) published by Ontario Ministry of Transportation (MTO) and Bridge Inspector's Reference Manual [15] published by U.S. Department of Transportation provides detailed guidelines for bridge inspection procedures. The MTO has provided valuable contribution to develop Bridge Condition Index (BCI). The BCI is based on the remaining economic worth of bridge. The OSIM describes four condition states of materials including: excellent; good; fair and poor. The inspector is required to record the quantities (area, length or units) of the bridge elements in each condition state. The recorded quantities can be used to calculate Bridge Element Condition Index (BECI) based on the remaining value of the deteriorating element. The Bridge Element Condition Index varies from 0 to 100, where 100 is the best condition. The BECI is calculated using Eq. 2. [10]. The BECI for all the elements are then used to calculate the overall Bridge Condition Index (BCI).

$$BECI = \frac{Current\ Element\ Value}{Initial\ Element\ Value} * 100 \qquad \text{Eq. 2}$$

In the UK, at national level, Bridge Condition Index (BCI) is used to quantitatively specify the condition of bridges [22], [7]. Blakelock et al (1998) introduced the idea that BCI should accord with the opinion of an experienced bridge inspector, if he inspects the bridge. The BCI ranges from 0 to 100, where 100 is described as new. In Australia, guidelines of AASHTO are the main source of the inspection methods. These are modified according to the local conditions. An Element Structural Condition Index (ESCI) is introduced to describe the condition of structural elements. This ESIC is used to calculate the Overall Structural Condition Index (OSCI). Additionally, OSCI also depends on the importance of elements, material vulnerability and number of element types. The OSCI is number from 1 to 4, where 4 is the worst condition and 1 represents the new bridge [21]. Omar et al. (2017) proposed bridge deck condition index (BDCI), which only indicates the condition of concrete bridge deck. Infrared thermography, ground penetration radar and visual inspection along with

fuzzy logic were used to develop BDCI. Aflatooni et al (2014) incorporated critical factors like environmental effects, floods, earthquakes, wind, vehicle impact along with live load to develop synthetic rating equations for bridges. Table 3 summarizes some of the current and previous indices/ scales used to rate bridges.

Caner et al (2008) inspected 28 bridges in Turkey to propose a simple method for the prediction of expected life of such bridges which are not inspected on periodic bases. This method is solely based on visual inspection and may be applicable in country like Pakistan, where bridge inspection is carried out on when-required bases.

Table 3. Summary of Few Present and Past Indices/ Scales used around the Globe

Country/ State	Index / Scale Used	Basis
U.K	Bridge Condition Index *(BCI)*	–
Australia	Overall Structural Condition Index *(OSCI)*	Based on element structural condition index
Ontario	Bridge Condition Index *(BCI)*	Based on remaining economic worth
New York	Bridge Condition Rating *(BCR)*	–
Japan	Deterioration Level *I to V*	Deficiency rating based on defects
Russia	Rating scale 1 to 3	–
Pakistan (Proposed)	Bridge Performance Index *(BPI)*	Based on weighted element condition rating

1.2 Description of Study Bridges

Bridge A is located on The Mall Road in the city of Lahore near Fortress Stadium. It goes over the railway track connecting the cities of Lahore and Karachi (Fig 1a). It is a reinforced concrete girder bridge constructed back in 1974 by Punjab Highway Department. Bridge carries two-way traffic, with a total of 59 spans. Span length varies from 4.5 m to 29 m, with maximum span over the railway track. Overall length of the bridge is 600 m and width is 10.5 m with the bridge skew of 38.25^{o}.
Bridge B is located on Jail Road in Lahore Cantt near the Cantt Railway Station (Fig 1b). This bridge was also constructed in 1974. It consists of two divided carriageways with a total length of 915 m, and width of 11 m. The bridge has 33 spans, with span length varying from 7.5 m to 30 m. It consists of prestressed girders with rectangular piers and non-prismatic RCC pier cap. Bridge has a skew of 36^{o}. In the year 2000, the bridge was widened and two lanes were added.

Fig 1 A. Study Bridge A

Fig 1 B. Study Bridge B

2. Methodology

The objective of the field work was to record the level of deteriorations and gather element condition rating data for both the bridges, which have consumed more than half of their service lives. Both bridges were inspected at the element level using the general condition ratings recommended by FHWA [14]. First step was to carry out reconnaissance of the bridges and the surroundings to identify the constraints and resources required to finish the work. Then, the crew was taken to the sites to verify the dimensions of various elements of the bridges. Based on the measured dimension, as-built drawings of both bridges were developed. It was revealed that the drawings of the bridges available

with government agency were significantly different from the structures on ground. Condition rating of a bridge primarily depends on the accuracy of its physical record, therefore, dimensional verification was an important step. An inspection form was developed to gather the field data and information.

Element condition rating data were recorded for the wearing surface, railing and barrier, expansion joints, drainage system, primary members (RCC and prestressed girders), diaphragms, deck slabs, bearing system, pier caps, piers, abutments and sidewalk. Each element of every span was rated (0 to 9) and total inspected area/ length/ number and damaged area/ length/ number were also recorded. The rating data were later used to calculate the Bridge Performance Index (BPI). Percentage deterioration is an additional information at this point and is not used to establish the element rating or to calculate BPI. May be in future, this information can become a part of element rating and BPI calculations. Table 4 provides the summary of the total inspected and deteriorated quantities for all the spans of both the bridges. The process of calculating BPI is presented in Fig 2.

Table 4. Summary of Inspected Quantities, Deteriorated Quantities and Average Condition Ratings

Element	Bridge *A*				Bridge *B*			
	Total Quantity Inspected	**Deteriorated Quantity**	**% Deterioration**	**Average Condition Rating** (All Spans)	**Total Quantity Inspected**	**Deteriorated Quantity**	**% Deterioration**	**Average Condition Rating** (All Spans)
Railing	1528.8 m^2	114.6 m^2	7.5%	7	2509.7 m^2	74.4 m^2	3.0%	7
Sidewalk	2286.2 m^2	191.3 m^2	8.4%	6	No Sidewalk		0.0%	N
Wearing Surface	10245.5 m^2	214.2 m^2	2.1%	8	15883 m^2	325.8 m^2	2.1%	8
Expansion Joint	122 Nos.	30 Nos.	24.6%	5	35 Nos.	20 Nos.	55.0%	4
Drainage	236 Nos.	60 Nos.	25.4%	5	163 Nos.	40 Nos.	25.0%	5
Deck	11782.3 m^2	237.4 m^2	2.0%	8	16804.8 m^2	363 m^2	2.2%	7
Girders	8797.0 m^2	184.8 m^2	2.1%	8	13384.9 m^2	283.1 m^2	2.1%	8
Diaphragm	2302.9 m^2	49.7 m^2	2.2%	8	1325.2 m^2	78.6 m^2	5.9%	7
Bearings	960 Nos.	633 Nos.	66.0%	4	528 Nos.	95 Nos.	18.0%	6
Pier and pied Cap	200.7 m^2	10.5 m^2	5.3%	7	1137.8 m^2	48.7 m^2	4.3%	8
Abutment	78.1 m^2	5.0 m^2	6.4%	7	60.3 m^2	3 m^2	4.9%	8

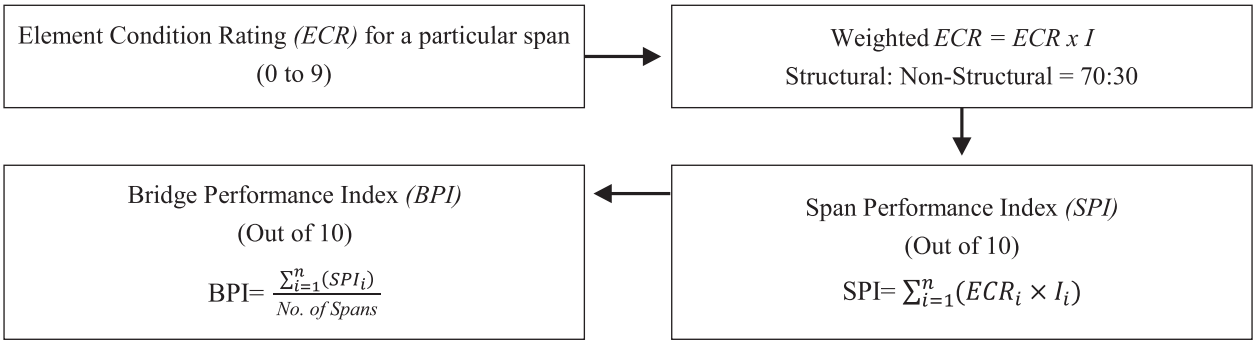

Fig 2. Process of Calculating BPI

2.1 Condition of Bridge *A*

Table 4 provides the average condition ratings of all the element of both bridges. Bridge *A* had 1.3 m high and 180 mm thick RCC railing. It had three posts, one in the mid and two at the ends. The thickness of the railing at the post was 250 mm. Railing in most of the spans was in very good condition with graffiti on the surface. Its soundness was checked with hammer. The average condition rating for all spans was found as 7, which indicates that railing only needs minor maintenance. The sidewalk was 1.5 m wide and was finished with tiles. In majority of the spans the level of the tiles was uneven with cracked tiles at several locations. Due to unevenness, rain water had been ponding, causing efflorescence in tiles. Sidewalk needs major maintenance. Wearing Surface was in very good condition, not requiring any repair. It seemed to have been recently laid. The curb that should be 275 mm high, was now only 125 mm, which reveals that re-surfacing was carried out twice. It also tells that the older wearing surface was not scarped before laying the new one. There were no potholes, no raveling or patching of the surface. Bridge had concealed expansion joints which are mostly employed for short spans bridge. Due to poor maintenance, 25% of the joints had worn out. Rain water had been penetrating through them to the structural elements beneath the deck (Fig 3). Drain pipes were 75 mm in diameter. Many of the drain pipes were clogged. Additional wearing surfaces had also blocked some of the drains. One of the leading causes of efflorescence in the super structure was the ponding of rain water due to full or partial clogging of drain pipes (Fig 4). Bottom surface of the deck was in good condition, except near the expansion joints as shown in Fig 5a. It was due to rain water penetration and ponding which caused efflorescence and delamination of concrete adjacent to the expansion joint. Span 6 of city-bound roadway was most severely damaged. Corrosion of reinforcement was also observed near the edges. When an edge of the deck was hammered, concrete broke off, showing rust marks of steel and indicating the loss of bond between reinforcement and deck concrete (Fig 5b). Top surface of deck was inaccessible due to wearing surface. Girders of Bridge *A* were in very good condition. Each roadway was composed of eight RCC girders, which had no structural cracks. The spans over railway crossing comprised of post-tensioned girders. Although girders appeared to be in very good condition, it is expected that rain water can harm the concrete and corrode the pre-stressing steel due to leakage from the worn out expansion joints and blocked drains. Each span had three RCC diaphragms, one at the mid and two at the ends. Light to moderate efflorescence and delamination was observed in the end diaphragms due to leakage of water from the expansion joints as shown in Fig 6. Other than this, the overall condition was good. Bearings in Bridge *A* were in most critical condition. Most of the bearings had jammed, particularly on the city bound roadway. Due to jamming of the bearing, as shown in Fig 7, local cracking and crushing of concrete in the pier cap was observed. Bearing system has lost its function and needs immediate replacement. Each roadway of Bridge *A* was supported on rectangular piers of size 1000 mm x 600 mm and a hammer head type pier cap. Light to moderate scaling was observed in the piers near railway spans. It may be due to weathering action and stagnation of rain water at the pier base. It had led to separation of concrete cover at some places. Pier caps had florescence at several locations, which was due to leakage of rain water through the worn out expansion joints.

(a) Cracked Wearing Surface at the Expansion Joint of Bridge A

(b) Water Leakage from Expansion Joint of Bridge A

(c) Worn Out Expansion Joint of Bridge B

(d) Water Leakage from Expansion Joint of Bridge B

Fig 3. Condition of Expansion Joints

(a) Choked Drain of Bridge A

(b) Stagnant Rainwater on Bridge B

Fig 4. Condition of Drainage System

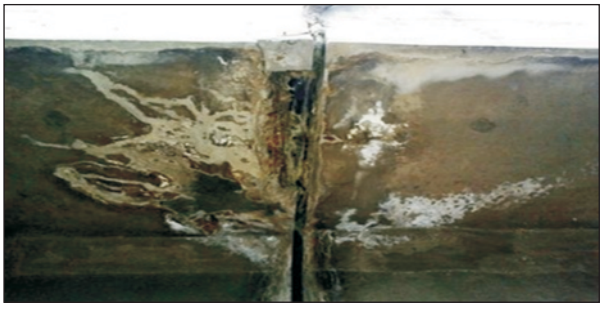

a) Deteriorated Deck near Expansion Joint

(b) Broken Piece of Deck

Fig 5. Condition of Deck of Bridge A

Fig 6. Deterioration of End Diaphragm of Bridge A

(a) Bearing and Pier Cap of Bridge A (b) Bearing of Bridge B

Fig 7. Condition of Bearings and Pier Cap

2.2 Condition of Bridge *B*

Bridge *B* had 1.1 m high New Jersey barrier with 600 mm high guard rail fixed on top. In general, barriers were in good condition. However there were collision marks on the barriers at few locations. Over speeding vehicles slide by the central and the end barriers. Due to vehicle collision, the pipe railing had broken at some places, particularly near the curved portion of the bridge. Central barrier has developed vegetation at some places particularly near light poles. There was no sidewalk in Bridge *B* at present. Previously, there were 1.2 m wide sidewalks on both sides, however after widening of the bridge, sidewalks became part of the drive way. Wearing surface of the bridge was in very good condition. However, at the interface of the old and the new structure a longitudinal crack spanning over the entire bridge length was observed. There were no potholes, no raveling or patching of the surface. Expansion joints of Bridge *B* had worn out severely (Fig 4). These joints cause noise when vehicles pass over them. Almost 100 mm deep cavity was observed in the joint space. Water had been leaking causing efflorescence in the superstructure. Expansion joints need immediate attention and would require major rehabilitation. Drainage condition in case of Bridge *B* was not different from Bridge *A*. Rainwater remains stagnant on the curved portion of the city bound roadway due to the clogging of drain pipes, as shown in Fig 4. Old portion was severely damp due to improper drainage created after remodeling of the bridge. Water coming down from drain pipes remains stagnant near the columns base and can cause damage to foundations. The condition of the deck was better compared to Bridge *A*. Light to moderate dampness was observed in some spans. Girders in Bridge *B* were prestressed. Each roadway consists of four post-tensioned girders, which were in good condition. No structural cracks or spalling were observed. Each span had three RCC diaphragms; one at mid and two at ends. Diaphragms were in good condition. Bearings of Bridge *B* were working better as compared to Bridge *A* (Fig 7). Steel plates with elastomeric neoprene pads were used, which had slight rusting of plate in some spans and deformations in the neoprene pads at some locations. Square piers of size 1.5 m x 1.5 m were used in the regular spans and rectangular piers in the railway spans. Both piers and pier caps were in very good condition. No loss of cover or structural cracks were observed in the inspection of piers. However, some cracks were observed in the pier cap underneath one of the exterior girders in the railway spans of the Cantt bound roadway.

2.3 Damage Patterns

Based on the condition rating of all the bridge elements, a comparison was plotted as shown in Fig 8. It can be seen that expansion joints, drainage, and bearings are the most deteriorated elements as compared to others. This trend reveals that maintenance agencies care more about the structural elements than the non-structural elements. Rainwater ponding and leakage due to unhealthy condition of non-structural elements can

cause harm to the health of primary structural elements. In addition to this, because the deterioration of bearings is not visible therefore they do not catch attention. This needs to be changed.

These damage patterns emphasize that the frequency of inspection of bridges in Pakistan should be based on the extent/ rate of damage of elements and the maintenance practices in the country, not on a pre-decided fixed interval. Maintenance of these bridge elements may not require huge financial resources, however, awareness about the periodic inspection and maintenance needs to be spread.

2.4 Bridge Performance Index (*BPI*)

Bridge Performance Index is an index proposed to indicate the condition of bridges in Pakistan. It ranges from 0 to 10 and is based on the condition of structural and non-structural elements. This index is based on condition rating of individual elements, and is a quantitative way of expressing the condition of bridge. An index like *BPI* can be made very elaborate or even complex, however, it is deliberately kept simple, keeping in view the nascence of the concept in the country. A quantitative way is adopted, which is easy to explain to the stakeholders, who are not always technical people. In future, *BPI* may be helpful for the government funding agencies to make decisions related to the budget allocations for bridge maintenance.

In developing *BPI*, 70% importance is assigned to the structural elements and 30% to non-structural elements of the bridge. Because the non-structural elements, specially drainage and expansion joints, seriously affect the condition of structural elements, therefore, non-structural elements deserve reasonable importance. The importance factors assigned to various elements are based on the consultations with experienced local bridge maintenance and design engineers. These weights can be modified as the index gets mature with time and by incorporating data of more bridges. Table 5 provides the Importance Factors (*I*) of all the 279 elements.

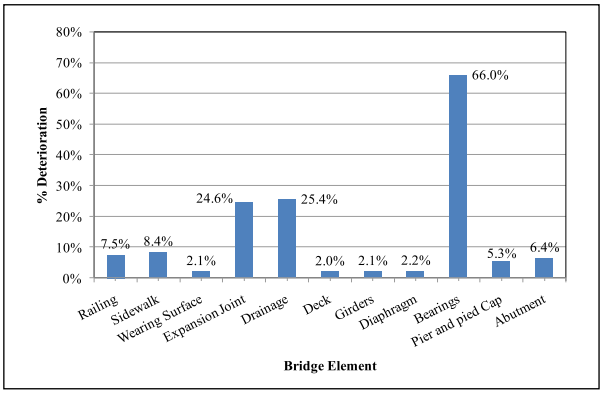

a) Bridge A

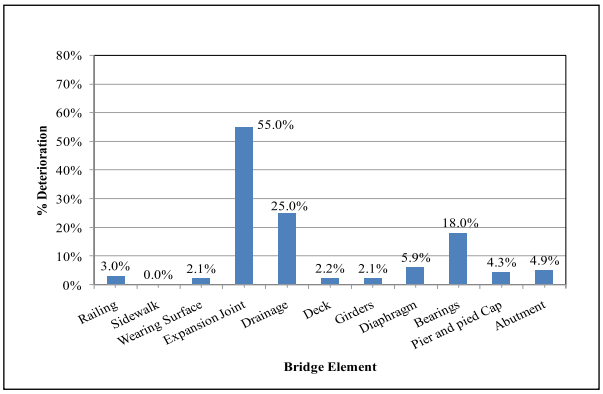

b) Bridge B

Fig 8. Damage Pattern of Study Bridges

Table 5. Calculations of Span Performance Index

Nature	Element	Importance Factor	Bridge A Span 1		Bridge B Span 1	
		I	*ECR*	*ECR x I*	*ECR*	*ECR x I*
Structural Elements	Deck	15%	8	1.2	8	1.2
	Girders	15%	8	1.2	8	1.2
	Diaphragms	5%	8	0.4	7	0.35
	Bearings	10%	4	0.4	6	0.6
	Piers and Pier Caps	20%	7	1.4	8	1.6
	Abutment	5%	7	0.35	8	0.4
	Sum	**70%**		**4.95**		**5.35**
Non-Structural Elements	Drainage	10%	5	0.5	5	0.5
	Expansion Joint	10%	5	0.5	4	0.4
	Wearing Surface	5%	8	0.4	8	0.4
	Railing/Barriers	3%	7	0.21	7	0.21
	Side Walks	2%	6	0.12	9	0.18
	Sum	**30%**		**1.73**		**1.69**
			SPI	**6.68**	***SPI***	**7.04**

Condition rating of each element of every span was carried out and then based on these raw data. Span Performance Index (*SPI*) for each span was calculated. The *SPI* is the summation of the products of Element Condition Rating (*ECR*) for the elements in a particular span and the importance factor (*I*) of the respective element (Eq. 3). Table 5 presents the calculation of *SPIs* for Span 1 of Bridges *A* and *B*. It is worthwhile to calculate the performance index at the span level because it will help identifying the problematic span. The model presented by Yanev (1997) calculates the overall condition index of the bridge which cannot identify the damaged span. The *SPIs* of all the spans are integrated into *BPI* of the entire bridge by calculating the average of all *SPIs* (Eq. 4). The SPIs of all the spans for both the bridges are presented in Table 6. The *BPI* is proposed as a multiple of 0.5, rounded to the lower side. The *BPIs* for both the bridges came out to be 7, indicating that both fall in the very good category, requiring minor repair only. If the weightages of structural to non-structural elements are changed to 65:35 or 75:25, *BPI* values for both bridges vary only within 0.5. Greater variation may however be 293 observed for bridges having structural elements badly deteriorated than non-structural elements 294 and vice versa.

$$\text{SPI} = \sum_{i=1}^{n} (ECR_i \times I_i) \qquad \text{Eq. 3}$$

$$\text{BPI} = \frac{\sum_{i=1}^{n} (SPI_i)}{n} \qquad \text{Eq.4}$$

Table 7 presents the proposed relation between the *BPI* and the condition of the bridge. It is worth mentioning that *BPI* can provide an idea of the overall condition of bridge, however, it cannot explicitly identify the member which has a localized severe damage. It is therefore necessary that while inspecting the bridge, the inspector must note down the location and extent of specific troubled area and indicate in his inspection forms the urgency to address that issue. It is recommended that if *BPI* falls below 4, the bridge should be closed for service till the rehabilitation is completed.

Table 6. Summary of Span Performance Indices (SPI)

Span No.	Bridge *A*	Bridge *B*	Span No.	Bridge *A*	Bridge *B*	Span No.	Bridge *A*
	SPI	***SPI***		***SPI***	***SPI***		***SPI***
1	6.68	7.04	21	7.64	6.26	41	6.88
2	6	6.54	22	8.21	7.56	42	6.36
3	7.43	7.13	23	8.41	7.83	43	7.35
4	6.35	6.87	24	6.56	8.27	44	8.11
5	8.12	7.86	25	6.96	6.37	45	7.25
6	6.37	6.73	26	7.56	7.25	46	6.73
7	8.54	7.23	27	6.25	6.73	47	7.84
8	8.75	8.43	28	8.36	7.37	48	6.73
9	7.01	7.37	29	7.73	8.63	49	8.55
10	6.46	8.36	30	8.26	7.35	50	6.34
11	8.19	6.03	31	7.27	7.22	51	6.78
12	6.98	8.55	32	8.93	6.34	52	6.34
13	6.45	7.39	33	6.26	7.88	53	8.53
14	7.84	6.18	34	7.17	-	54	7.36
15	8.14	7.83	35	8.34	-	55	7.35
16	8.76	8.59	36	7.36	-	56	6.22
17	8.16	6.83	37	6.17	-	57	6.73
18	7.56	8.77	38	8.52	-	58	7.83
19	8.6	6.35	39	7.28	-	59	6.26
20	6.74	7.09	40	6.73	-		

Table 7. Qualitative Expression of BPI

***BPI* Range**	**Condition of Bridge**	**Action Recommended**
$8 < BPI \leq 10$	Excellent	No Repair Needed
$6 < BPI \leq 8$	Very Good	Minor Repair
$4 < BPI \leq 6$	Good	Major Repair
$2 < BPI \leq 4$	Poor	Minor Rehabilitation
$BPI \leq 2$	Dangerous	Major Rehabilitation or Decommission

3. Summary and Conclusions

This work was focused on performing condition rating of two highway bridges situated in the city of Lahore, Pakistan and calling attention to the need of adopting proactive approach for maintenance of bridges. The basic concept of Bridge Performance Index (*BPI*) is proposed with more refinement by using data of larger stock of bridges. The incorporation of non-destructive testing, may be used to indicate the condition of bridges and prioritizing repair and rehabilitation projects in Pakistan. Utilization of public money for maintaining bridges may be optimized, both in terms of time and place by using *BPI* and the savings may be channelized in the right direction for infrastructure development and maintenance.

Based on visual inspection, all the elements were rated on a scale of 0 to 9, as recommended by the FHWA (1995). Structural elements of both bridge were in good condition however, non-structural elements like expansion joints, bearings, and drain pipe were in poor condition. The deterioration seen

at several places in structural elements was mainly because of improper functioning of non-structural elements. High deterioration in the non-structural elements points towards tendency of the maintenance agencies to ignore the non-structural elements and any element which is not visible from outside. In fact, the hidden elements should be given due importance. The raw data of element condition rating (*ECR*) were used to compute the span performance index (*SPI*) and subsequently the *BPI*. The *BPI* provides information about the overall condition of the bridge, however it cannot identify a specific element which has structural health issues. It is the responsibility of bridge inspector to state in the inspection form the location and extent of any severe problem. The *SPI* however, may help in identifying the problematic span. It is recommended that if *BPI* of a bridge falls below 4, it should be closed for service and immediate action of rehabilitation should be carried out. The *BPI* of both Bridges came out as 7 on the scale of 10, which means that both bridges fall in the *very good* category and require only minor repair. This result is consistent with the judgment made by the inspector during the field inspection. Blakelock (1998) suggested that the condition index and the observation of an experienced bridge inspector should be consistent with each other. In future, it may be a good idea to combine the condition of bridge and importance of bridge in the road network in the calculation of *BPI*, as does the bridge condition index of South Africa [16]. There is a need to create a database of *BPIs* for the entire bridge inventory of Pakistan, which can be used to develop bridge management system (BMS) for the country. Implementation of an integrated BMS at the national or at least at the provincial level may help in timely addressing most of the issues related to the health of bridges.

4. Recommendations

In the light of the observations made during the field work, following recommendations are made for the various highway agencies in Pakistan:

1. Given the circumstances in the country, the frequency of Inspection should be decided based on the condition of the bridge and environmental/ geographical conditions but not exceeding a fixed cycle of 2 years. This limiting time of 2 years may be changed based on the observation of several inspection cycles. Risk based inspection (RBI) method [25] may also be a suitable choice to decide the inspection interval
2. Based on the field observations, it is recommended that drainage system must be inspected and flushed at least once a year before the rainy season. Expansion Joints should also be inspected once a year and bearing system after every 2 years. Due to serious durability issues of expansion joints in Pakistan, troughs should always be provided at the location of these joints which could collect rainwater and discharge it into a downpour. Alternatively, expansion joints must be properly sealed and seals should be replaced periodically.
3. It was observed that in Bridge *B*, new wearing surface was laid without scraping the older one. This practice reduces the live load capacity of the bridge and compromises the safety of the pedestrians using sidewalk. Such practice should be strictly prohibited.
4. Aged bridges located in the seismic regions should be tested to determine their dynamic response. For such bridges, dynamic characteristics may also become a part of performance index.
5. For the bridges with low BPI, non-destructive testing and structural health monitoring may be considered as advanced options to make decisions on repair/ retrofit/ reconstruction.
6. If one government agency constructs a bridge and its maintenance is carried out by another agency, the first agency should be provided with complete data of repair/ rehabilitation for record upkeep. It is strongly recommended that a bridge should be taken care of by the same agency throughout its service life.

Acknowledgements

Authors would like to acknowledge the support of Bridge Engineering Laboratory, Department of Civil Engineering, University of Engineering and Technology, Lahore, Pakistan.

References

[1] AASHTO. (1970). "Manual for Maintenance Inspection of Bridges", Washington, DC.

[2] AASHTO. (2011). "Guide Manual for Bridge Element Inspection". Washington, DC.

[3] ASCE/SEI-AASHTO Ad-Hoc Group. (2009). "White Paper Paper on Bridge Inspection and Rating." *Journal of Bridge Engineering*, 2009, 14(1): 1-5.

[4] ASCE. (2017). "Infrastructure Report Card" Alexander Bell Drive, Reston, VA.

[5] Aflatooni, M., Chan, T.H.T., and Thambiratnam, D.P. (2014). "Synthetic Rating Procedures for Railway Bridges." Journal of Bridge Engineering, 19(12).

[6] Bektas, B. A. (2011). "Bridge Management from Data to Policy." *PhD Dissertation*, Iowa State, University, Ames, Iowa.

[7] Blakelock, R., Day, W., and Chadwick, R. (1998). "Bridge Condition Index: The Management of Highway Structures." Highway Agency, Surrey, UK.

[8] Brodsky, G., Muzykin, R., Brodskaia, E., Ponomarev, Yu., Yenyutin, Yu., and Vlasova, M. (2006). "Analysis of Parameters of Structure Deterioration Models within the Moscow Bridge Management System." *Structure and Infrastructure Engineering*, Taylor & Francis, 2(1), 13-21.

[9] Caner, A., Yanmaz, A. M., Yakut, A., Avsar, O., and Yilmaz, T. (2008). "Service Life Assessment of Existing Highway Bridges with No Planned Regular Inspections." *Journal of Performance of Constructed Facilities*, 22(2), 108–114.

[10] Dabous, S. A. (2008). "Unified Condition Index for Existing Concrete Bridges in Canada." *Proc., Canadian Transportation Research Forum 43rd Annual Conference*, New Brunswick, Canada.

[11] Elbehairy, H. (2007). "Bridge Management System with Integrated Life Cycle Cost Optimization." *PhD Dissertation*, University of Waterloo, Waterloo, ON, Canada.

[12] Elbeltagi, E., Elbehairy, H., Hegazy, T., and Grierson, D. (2005). "Evolutionary Algorithms for Optimizing Bridge Deck Rehabilitation." *Proc., Int. Conf. on Computing in Civil Engineering*, ASCE, Reston, Va., 619–630.

[13] FHWA. (1971). *National Bridge Inspection Standards*, Washington, DC.

[14] FHWA. (1995). *Recording and Coding Guide*, Washington, DC.

[15] FHWA. (2012). *Bridge Inspector's Reference Manual*, Washington, DC.

[16] Hooks, J., and Frangopol, D. M. (2013). "LTBP Bridge Performance Primer." FHWA-HRT-13-051, Federal Highway Administration, Washington, DC.

[17] Liu, C., Hammad, A., and Itoh,Y. (1997). "Multi-Objective Optimization of Bridge Deck Rehabilitation Using Genetic Algorithm." *Journal of Computer-Aided Civil and Infrastructure Engineering*, 12 (6), 431-443.

[18] New York DOT. (2014). Bridge Inspection Manual, Albany, NY.

[19] Ontario Ministry of Transportation. (2000). "Ontario structure inspection manual." Ontario, Canada.

[20] Omar, T., Nehdi, M.L., and Zayed, T. (2017). "Integrated Condition Rating Model for Reinforced Concrete Bridge Decks" Journal of Performance of Constructed Facilities., 10.1061/(ASCE)CF.1943-5509.0001084.

[21] Rashidi, M., and Gibson, P. (2012). "A methodology for bridge condition evaluation." *Journal of Civil Engineering and Architecture*, 6 (9), 1149-1157.

[22] Ryall, M. J. (2001). "*Bridge Management.*" Butterworth-Heinemann, Oxford, UK.

[23] Texas Department of Transportation. (2002). *Bridge Inspection Manual*, Austin, TX.

[24] Turner, A., and Richardson, J. (1994). "Bridge management system data needs and data collection." *Transportation Research Circular*, 423, TRB, pp. 5-15.

[25] Washer, G., Connor, R., Nasrollahi, M., and Provines, J., (2015). "New Framework for Risk-Based Inspection of Highway Bridges" Journal of Bridge Engineering.,10.1061/(ASCE)BE.19435592.0000818.

[26] Washer, G., Connor, R., Nasrollahi, M., and Reising, R. (2016). "Verification of the Framework for Risk-Based Bridge Inspection" Journal of Bridge Engineering., 10.1061/(ASCE) BE.19435592.0000787.

[27] Yanev, B. (1997). "Life-cycle performance of bridge components in New York City." *Proc., Recent Advances in Bridge Engineering*, Zurich, Switzerland, 385–392.

[28] Yanev, B. S. (2005). "Bridges: Structural Condition Assessment." John Wiley & Sons Inc., Hoboken, NJ.

[29] Yokoyama, K., Sato, H., Ogihara, K., and Toriumi, R. (1996). "*Development of a bridge management system in Japan*." *Proc., Third International Conference on Bridge Management*, Surrey, UK., 580-586.

[30] Zhang, C., Zayed, T., and Hammad, A. (2008). "Resource Management of Bridge Deck Rehabilitation: Jacques Cartier Bridge Case Study.*" Journal of Construction Engineering and Management*, 134(5), 311–319.

ISSN NO. 2706-9648

Pakistan Journal of Engineering

For online access, please visit:
journal.pec.org.pk

DEVELOPMENT, CHARACTERIZATION AND APPLICATION OF TRANSPARENT SUPER-HYDROPHOBIC SURFACE COATINGS

Shahid Hussain Abro, Alidad Chandio, Sania Aslam

ARTICLE INFO

Article History:

Accepted 16 Oct 2020

Published on 25 Oct 2020

Keywords

Sol-gel; hydrophobic; water-repellent; contact angle; adhesion; corrosion resistance; hardness.

ABSTRACT

Amongst several types of hydrophobic coatings; transparent hydrophobic coatings are highly preferred due to their water repellant, self-cleaning and anti-reflective nature with ideally having contact angle greater than 90°. These coatings can be prepared in various forms but in particular silica-based coatings are most effective as they are inexpensive, environmentally friendly, and versatile and can be applied on different substrates like, cloth, wood, glass, paper etc. The current study deals with sol-gel method to synthesize Silica based coatings, followed by grinding (mechanical polishing) of substrates in order to enhance contact angle and surface adhesion. The aim of this contribution is to develop better understanding of transparent super-hydrophobic coatings in addition to associated parameters such as types of substrates, variable roughness and annealing temperatures. The results demonstrate contact angle greater than 90° with surface roughness found to be having profound influence on contact angle in addition to enhanced adhesion. Effect of annealing temperature was also examined which resulted in the similar trend as of roughness. Moreover, the coated fabric samples exhibited improved resistance to wetting yet not sufficient enough at current level of investigation. Coated wood samples also showed considerable improvement in hardness.

1. Introduction

Living beings and plants have the ability of self-cleaning character inferable from the super hydrophobic surface. A hydrophobic by definition means “tending to repel or fail to mix with water”. Nonpolar molecules that repel the water molecules are said to be hydrophobic. The most meaningful delineation is the supposed lotus-impact (Neinhuis and Barthlott, 1997). The wettability of the surface

not just influences the essential development of the living life forms in nature yet in addition affects our day by day life. Late disclosures have connected the self-cleaning component of a lotus plant to a minute morphology prompting super hydrophobic surfaces [1-3]. This finding has started the enthusiasm of various specialists to build up a bio-mimetic way to create a similar impact [4-7]. The vision of generation of super hydrophobic surfaces has enormous potential applications in the area of corrosion restraint for metal parts, preparation and organic operator insurance for apparel, defensive coatings on windows, auto windshields, sun oriented boards, wind turbine edges and other expansive open air surfaces and numerous other mechanical and industrial applications. Keeping in mind the end goal to accomplish super hydrophobic surfaces like that of the lotus leaf, two elements, the surface morphology and surface science should be controlled at the same time. To accomplish powerful self-cleaning over a long stretch of administration time, these coatings must be mechanically strong with high imperviousness to wear and disintegration. Sol-gel innovation is the favored course to create such coatings [8-13]. Because the coveted properties of the coatings can be effectively balanced through formulation, including hardness, surface roughness, transparency, and surface energy, and so forth. The essential motivation behind taking a shot at this point was to expand surface roughness through various methodologies like piranha treatment, annealing and grinding, and to consider its impacts on glass. Impact of grinding on coated surface was likewise look at through this investigation by scratch test [14-20]. The washing cycle impact on coated fabric and its testing strategies were talked about in this investigation. The impact of corrosion resistance of covering on metals and effect of coating on wood swallowing property were additionally examined [21-23].

2. Materials and Methods

For sol-gel method, sol was prepared using 5ml Tetraethyl Orthosilicate (TEOS), 5ml Trimethyl-methoxysilane (TMMS) and 3grams of RTV silicone sealant in 20ml of ethanol. These ingredients were magnetically stirred at room temperature for 30 minutes. Thereafter, substrates were dipped into the solution and then oven dried at 70°C for 20 minutes. Moreover, Piranha solution was prepared by combining 75% H_2SO_4 and 25% H_2O_2 and applied onto the cleaned glass. The glass was then rinsed thoroughly by water followed by application of coating. Surface roughness of the glass substrates was varied using different grades of emery papers (Silicon carbide) papers of 180, 400, 600, 800, 1000 μm grit in order to analyze the effect of surface roughness on adhesion. Glass substrates were grounded using these grits both in lateral and longitudinal directions. Once surface roughening was complete, these substrates were coated. Afterwards, substrates were subjected to post treatment process i.e. annealing at different temperatures (100, 150 and 200 °C for 20 minutes each) in order to enhance adhesion.

Water droplet's contact angle on the coated substrates was measured using high definition picture by AutoCAD. Contact angle was determined by the average angle of the droplets dispensed at different locations of films. Scratch test was also carried out in order to determine adhesion of the coating by applying scratch on coated surface and length of scratch was examined by optical microscope. To find out the effects of washing on contact angle and hydrophobicity, washing cycle test was performed. There were 10, 20, 30, 40 and 50 spins executed with 1, 2, 3, 4 and 5 wash cycles, respectively. Linear polarization resistance (LPR) test was also carried out by using computerized potentiostate, in order to determine the effect of hydrophobic coating on corrosion behavior of metal substrate. Moreover, Hardness of wood in different conditions were tested by using shore D hardness scale.

3. Results and Discussion

3.1 Contact Angles on Different Substrates

A single drop of water was placed on the substrates and pictured via high definition (HD) Camera as shown in Fig 1. The contact angles on each of these substrates shown in Fig 1 were measured and shown graphically in Fig 2.

The contact angles measured were greater than 90° which showed that the coating is hydrophobic in nature and can be applicable for all substrates. The coating exhibited very low surface energy, which means that it is very difficult to wet consequently creating small mountains or hill and valley like structure on the surface. So when water droplet falls on the surface, it will be suspended on it and maintain an air gap between water and the surface. The different values of contact angle (see Fig 2) depicts that the difference between the surface free energy of coating and substrates are enormous as a result affecting the hydrophobic properties of the coating.

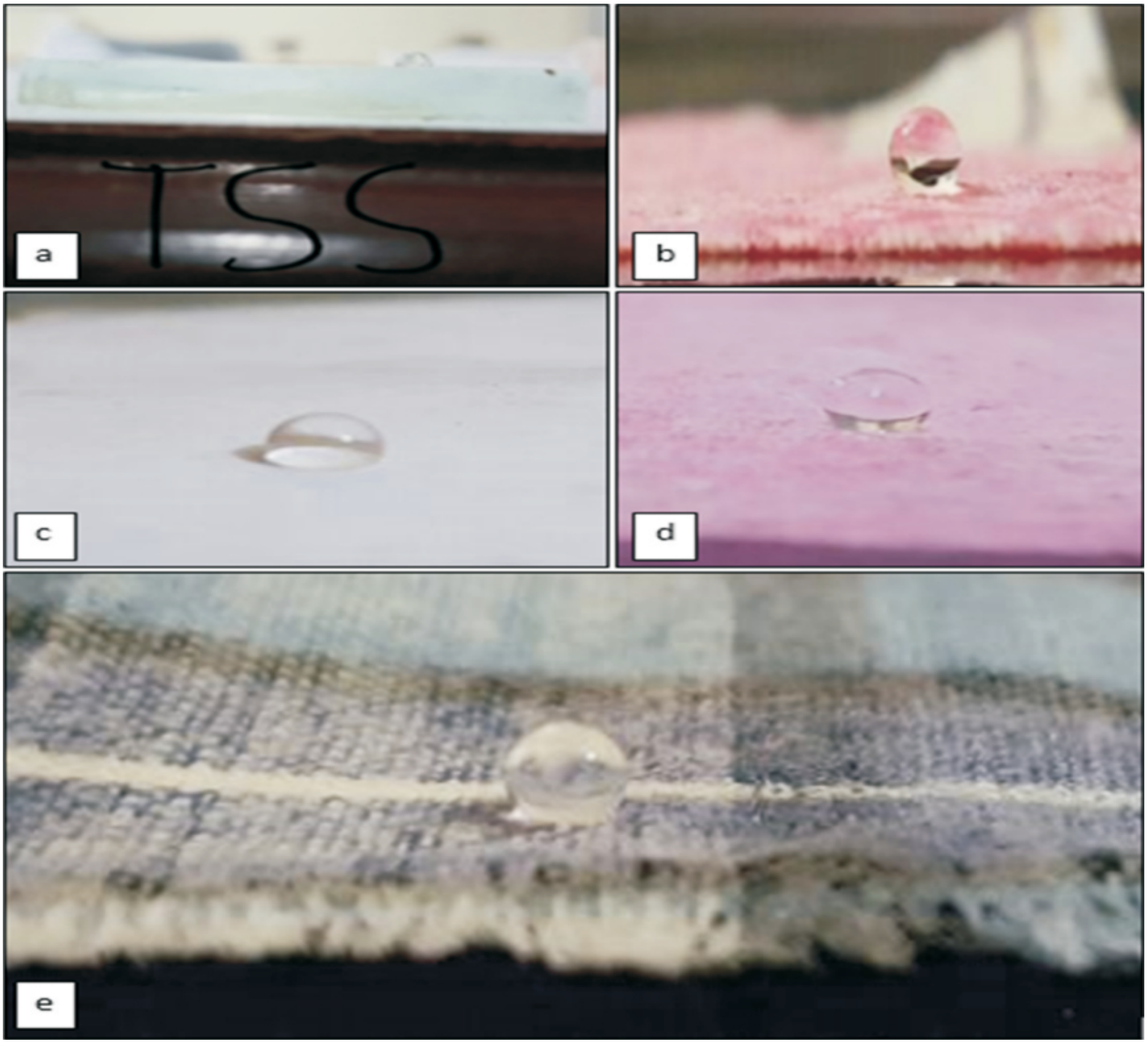

Fig 1. The water droplet on different substrates; (a) glass, (b) cotton, (c) normal printing paper, (d) tissue paper and (e) polyester cloth

3.2 Contact Angles at Different Roughness

Surface roughness was modified by grinding glasses at different grit sizes. It appeared very clear that surface roughness affects water contact angle (WCA) significantly, thereby affecting degree of hydrophobicity. With increased roughness of glass surface the contact angle also increases as shown in Fig 3. This effect is completely valid as per the theoretical aspect that by increasing surface roughness the surface energy decreases, and the bond between substrate and hydrophobic coating increases which enhances the water repelling effect of the coating.

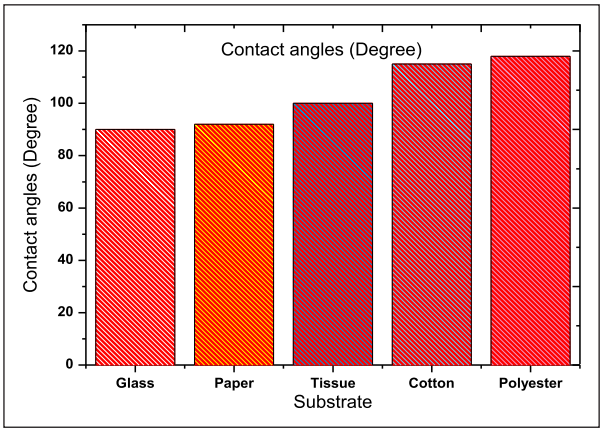

Fig 2. Depicts the measured values of contact angle of substrates

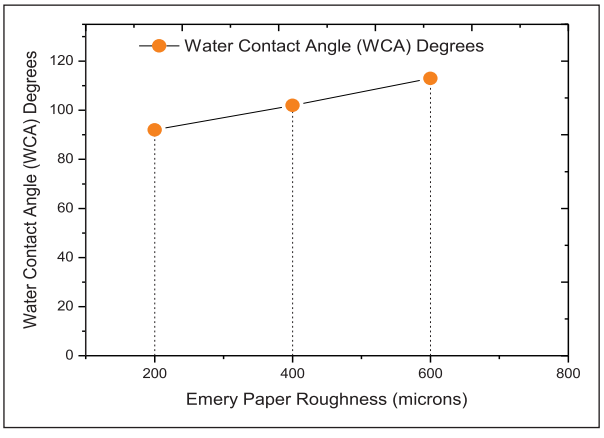

Fig 3. The effect of surface roughness on the contact angle of glass

3.3 Contact Angles after Annealing

The coated glasses were simply annealed at different temperatures to study the increasing temperature effect on behavior of hydrophobic coatings as depicted in Fig 4. It appears very clear that by increasing annealing temperature, the contact angle increases significantly, which means that at high temperatures upto 200 oC, the contact angle value is highest and the coating is not losing its effect of hydrophobicity on glass. This treatment has also proven beneficial in enhancing the coating adhesion.

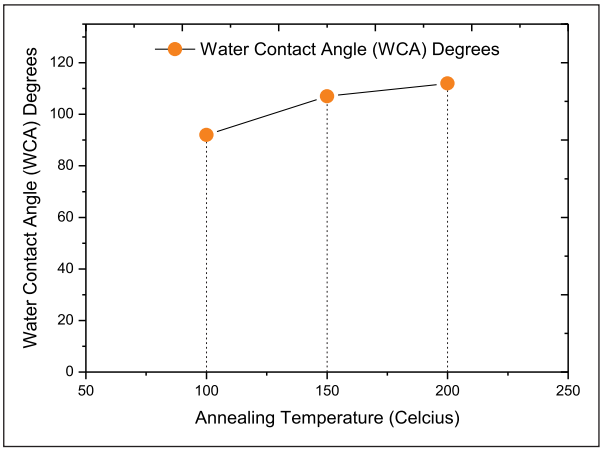

Fig 4. The effect of annealing treatment on the contact angle of glass

3.4 Effect of Washing

Washing cycle test was performed by manually spinning the fabric in detergent containing water. On the average of 10, 20, 30, 40 and 50 spins of washing, it appeared that there is no effect of washing on coated fabric as with increasing wash cycles, the hydrophobicity of fabric remains almost same (see Fig 5). However, observed slight differences were presumably attributed to calculation error because the fabric coated with hydrophobic coating, repels the water or at least hinders the wetting effect.

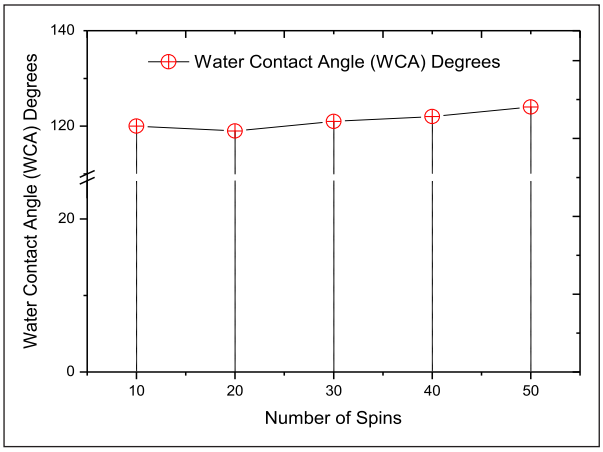

Fig 5. The effect of washing cycles on the contact angle of fabric

3.5 Adhesion

In order to understand the adhesion of hydrophobic coating, scratch testing was carried out (Fig 6). For grit size of 1000 microns, the following formula was used:

Chipping of length = total length – chipping of length (1)

Chipping of length=2077-1050=1027 x10^{3}mm (2)

While

Chipping failure = Edge chipping x 10 (Load/ distance ratio) + initial load (3)

Chipping failure = 1027 x 10^{-3} x 10 (60 / 2077 x 10^{-3}) +10.4 = 307.077 N (4)

Moreover, to further estimate the effect of surface roughness on adhesion, the scratch test was carried out on glass substrate of varying roughness as shown in Fig 7. It appeared that on increasing the roughness size grinding paper, it creates surface features resembling small mountains/ hills and valleys which have low surface energy as compared to its counterpart i.e. coating solution of glass substrate adhesion also increases. The reason to this is that when glass is sanded with different grit. Therefore, the difference between the surface energies gives good adhesion property. As a result, the bond strength is increased.

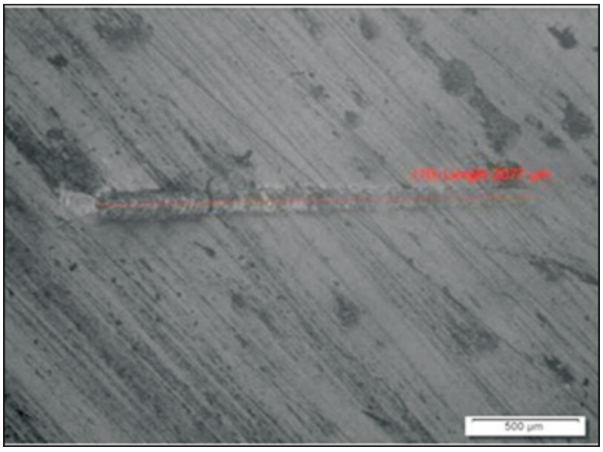

Fig 6. Result of scratch test on the glass sample at grit size of 1000 microns

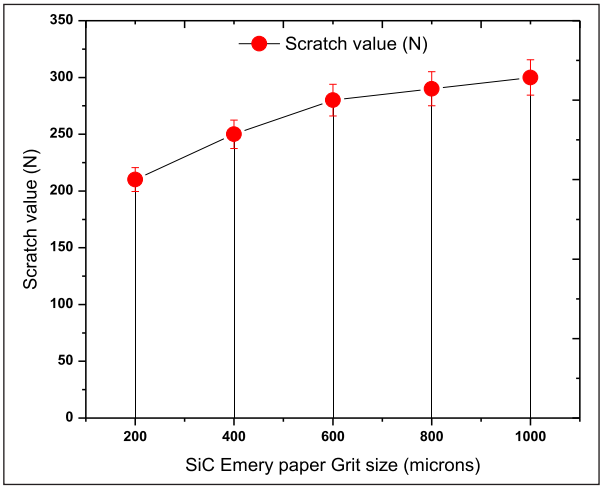

Fig 7. The adhesion test values at different surface roughness of the glass

3.6 Corrosion

Hydrophobic coatings provide anti-corrosive property on metal surfaces because a very small amount of it stays on the surface. In this connection, the corrosion test was performed and the results are presented in Table 1. The results show that the coated metal has less corrosion rate than that of its uncoated counterpart, and high resistive potential values for coated surfaces indicate coating exhibiting more resistance to corrosion. As

hydrophobic coating repels water and never allows the water to stay on metal surface. This reduces the electrical conductivity consequently protecting it from corrosion.

Table 1. shows the corrosion rates of coated and un-coated samples

Sample	Corrosion rate (mills per year)	Resistive potential (Ω)
Coated	1.69×10^{-07}	19.55
Un-coated	1.47×10^{-06}	2.252

3.7 Hardness

Hardness testing was carried out using Micro-Vickers hardness testing machine. Hardness is the resistance to indentation or deformation or scratch. Higher the hardness more the ability of the surface to resist the mechanical wear. In this case, the hardness of wood sample was determined. Fig 8 shows the effect of coating on hardness of wood substrate. Coated and uncoated samples were soaked in water; the hardness of uncoated soaked wood was measured to be low as compared to the hardness of coated soaked sample. This is because an uncoated sample absorbed water more readily than that of its coated counterpart.

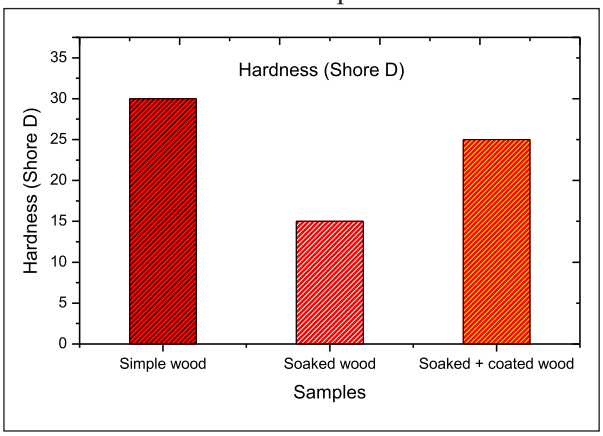

Fig 8. The hardness of coated and un-coated wood after soaking in water

4. Conclusion

Based on the results, it is concluded on the initial investigation of hydrophobic coatings that after application of the coating, measured contact angles were greater than 90° that exhibited hydrophobic nature of the coating, consequently corrosion resistance was increased significantly. Surface roughness was found to enhance the contact angle significantly in addition to enhanced adhesion. Similarly, the effect of annealing temperature on contact angles and adhesion were comparable to effect of surface roughness. Moreover, the coating fabric samples exhibited improved resistance to wetting but not sufficient enough at this initial investigation. Some of the wood samples were also subjected to hydrophobic coating. The hardness of uncoated soaked wood was measured to be low than that of the coated-soaked counterpart.

Acknowledgements

We would like to thank the staff of Materials and Metallurgical Engineering Department, NED University and Engineering Technology, Karachi for their valuable support and NED University for financial assistance.

References

[1] GURAV, A. B., LATTHE, S. S., KAPPENSTEIN, C., MUKHERJEE, S., RAO, A. V. & VHATKAR, R. S.. Porous water repellent silica coatings on glass by sol–gel method. Journal of Porous Materials, 2011; 18, 361-367.

[2] Choi, S.J. and HUH, S.Y. Direct Structuring of a Biomimetic Anti-Reflective, Self-Cleaning Surface for Light Harvesting in Organic Solar Cells. Macromolecular rapid communications: 1996; 31(3). 318-331.

[3] HOWARTER, J. A. & YOUNGBLOOD, J. P. Self-Cleaning and Next Generation Anti-Fog Surfaces and Coatings. Macromolecular Rapid Communications: 2002; 9, 455-466.

[4] Alidad Chandio, Shahid Hussain Abro, Effect of Temperature and Time on Nickel Aluminide Coating Deposition, Mehran University Research Journal of Engineering & Technology: 2018; 37, No. 4, 491-496.

[5] S. ISHTEYAQUE, S. JABEEN, S. H. ABRO, Hazard and Operability Study of Gas Exploration Field Located in Pakistan, Sindh University Research Journal-SURJ (Science Series): 2019; 51, 2, 189-194.

[6] Kashif Ali Abro, Anwer Ahmed Memonc, Shahid Hussain Abro, Enhancement of heat transfer rate of solar energy via rotating Jeffrey nanofluids using Caputo–Fabrizio fractional operator: An application to solar energy. Journal of Energy Reports: 2019; 5, 41-49.

[7] S. H.ABRO, A.A.SHAH, A. D. CHANDIO, R. BLUNDELL, Effect of Al, Ni, Mo, Ti, Nb and temperature on grain size number in low carbon high alloyed steel Sindh Univ. Res. Jour. (Sci. Ser.): 2018, l, 51,59-64.

[8] Shahid Hussain Abro, Syed Aqeel Ahmed Shah, Abdulaziz S Alaboodi, and Talha Shoaib Ageing Analysis of Power Cable used in Nuclear Power Plant Mehran University Research Journal of Engineering & Technology: 2020; 39, 1, 2413-7219.

[9] Shahid Hussain Abro et al, Influence of Austenite Phase Transformation on Existing Microstructure of Low C-Mn Steel. Engineering, Technology & Applied Science Research: 2018; 8, 6, 3525-3529.

[10] Ali Dad Chandio, Muhammad Basit Ansari, Shahid Hussain Abro, Silicon Carbide Effect as Reinforcement on Aluminum Metal Matrix Composite, J.Chem.Soc.Pak: 2019; 414, 20, 650-654.

[11] Shahid H. Abro, Alidad Chandio, Hazim. A.Moria, Findings of Grain Coarsening Temperature and Grain Growth of Light Weight Steel Used in Automotive Industry Pak. J. Egg. Appl. Sci: 2019; 25, 14-17.

[12] Shahid Hussain Abro, A Role of Mn atoms on tensile properties of light weight CHQ steel. Mehran University Research Journal of Engineering & Technology. Journal of Engineering and applied Sciences: 2019; 38,1, 201-209.

[13] Murtuza Mehdi, Maaz Akhtar, Shahid Abro, Electrochemical synthesis of AgNP and mechanical performance of AgNP-EG. Journal of Elastomers and Plastics: 2019; 1,11, 240-245.

[14] SH Abro, MS Hanif, F Hussain, On the Effect of γ-phase transformation kinetics upon microstructure response of Cold Heading Quality Steel, NUST Journal of Engineering Sciences: 2018; 11 (2), 51-55.

[15] Shahid Hussain Abro, Alidad chandio , Muhammad Ali Siddiqui , and Iftikhar A. Channa, uminum and Aluminum Nitrides Effect on Nucleation Sites in Micro-alloyed Steel, Proceedings of the Pakistan Academy of Sciences: Pakistan Academy of Sciences A. Physical and Computational Sciences: 2019; 56 (3), 1-10.

[16] Shahid Hussain Abro. Hazim Abdulaziz Moria et al, Understanding The Effect Of Aluminum Addition On Forming The Second Phase Particles On Grain Growth Of Micro-Alloyed Steel. Journal of Engineering, Technology & Applied Science Research: 2020 10, No. 1, 202-211.

[17] Shahid Hussain Abro, Alidad Chandio, Abdulaziz S. Alaboodi and Iftikhar Ahmed Channa, Role of Automotive Industry in Global Warming. Pak. j. sci. ind. res. Ser. A: phys. Sci: 2019, 62A (3), 197-201.

[18] Shahid Hussain Abro, Alidad Chandio, Umair Aftab Effect of Heating Rate on Microstructural Developments in Cold Heading Quality Steel used for Automotive Applications" Mehran University Research Journal of Engineering & Technology: 2018, 37, 3, 461-466.

[19] LATTHE, S. S., DHERE, S. L., KAPPENSTEIN, C., IMAI, H., GANESAN, V., RAO, A. V., WAGH, P. B. & GUPTA, S. C. Sliding behavior of water drops on sol–gel derived hydrophobic silica films. Applied Surface Science: 2010, 256, 3259-3264.

[20] MAHADIK, S. A., KAVALE, M. S., MUKHERJEE, S. & RAO, A. V. Transparent superhydrophobic silica coatings on glass by sol–gel method. Applied surface science: 2010; 257, 333-339.

[21] NEINHUIS, C. & BARTHLOTT, W. Characterization and distribution of water-repellent, self-cleaning plant surfaces. Annals of botany: 1997; 79, 667-677.

[22] YAO, X., SONG, Y. & JIANG, L. Applications of bio-inspired special wettable surfaces. Advanced Materials: 2011; 23, 719-734.

[23] ZHAO, N., XU, J., XIE, Q., WENG, L., GUO, X., ZHANG, X. & SHI, L. Fabrication of Biomimetic Superhydrophobic Coating with a Micro-Nano-Binary Structure. Macromolecular rapid communications: 2005; 26, 1075-1080.

ISSN NO. 2706-9648

Pakistan Journal of Engineering

For online access, please visit:
journal.pec.org.pk

DESIGN AND DEVELOPMENT OF HUMAN KNEE JOINT MUSCLE(S) CLASSIFICATION SYSTEM USING MACHINE LEARNING TECHNIQUE

Nadeem Shah, Abbas Khan, Hira Zahid, Ali Asghar, Dilawer Hussain, Ali Shan

ARTICLE INFO

Article History:

Accepted 16 Oct 2020

Published on 25 Oct 2020

Keywords

sEMG, Classification, knee Joint, SVM, Machine Learning, AI, Matlab.

ABSTRACT

This paper presents an automatic system to examine and evaluate the different leg movements based on sEMG (Surface Electromyogram) sensors blended with state-of-the art machine learning algorithms for the classification and recognition of defects in the muscle(s). The proposed system is intelligent enough to classify if there is any abnormality in the knee movement, the system will automatically classify which muscle(s) are affected. For the signal acquisition process 4 sensors were placed on hamstring (semitendinosus, biceps femoris) and quadriceps (vastus medialis, rectus femoris) muscles. Arduino-powered sEMG sensors, made by DFRobot and OYMotion, were used to analyze the behavior of muscles associated with the flexion and extension of the knee joint during walking, sitting and lying down. Twelve time-domain signals were collected (three exercises having four different signals representing each of the four muscles) for a different range of leg motions. These signals were then sent to MATLAB for further processing and feature extraction. In the next step, key features were combined to form twelve feature descriptors representing four muscles and three exercises, involving knee joint motion. Later, the data was divided into two categories of healthy and unhealthy data. A Support Vector Machine (SVM) which is a supervised machine learning algorithm, was used for the classification of the signals. The healthy and unhealthy data was then assigned with labels and presented to SVM for training and testing of the system. After the model was created, the application was designed by using the MATLAB that provides a Graphical User Interface (GUI) to the user. The final testing and performance of the system were verified from the k-fold cross-validation test (where k=5) and results show the remarkable performance of the system where classification accuracy was also 0000improved to 99% by increasing the number of features and the polynomial order of the SVM model.

1. Introduction

Electromyography (EMG) is a method used for measuring electrical signals generated by skeletal muscles having a lot of useful information about the muscle(s) condition [1]. The muscular system is responsible for different movements related to the human body. The bio-signals recorded are known as myoelectric or electromyogram. The pattern recognition system based on EMG has been extensively used in several aspects of biomedical applications, i.e. clinical diagnosis [2], rehabilitation robots [3], [4], assistive computers [4], [5], upper-limb and lower-limb prostheses [6], [7], wearable devices and powered exoskeletons [8]. EMG signals can be acquired either by using concentric needle electrodes or surface electrodes. Since the sEMG signal is deterministic and stochastic in nature [2] so it is recommended not to use it directly in prosthetic devices. In the last few years [9]–[13] it has become effectively practical to classify the sEMG signals recorded from upper limb muscles. However, not much work has been done on the lower limb muscles, thus the processing and classification of bio-signals acquired from the lower-limb muscles are open research, since the last decade.

Hamstring and quadriceps muscles are the agonistic muscles in knee flexion and extension movements, respectively [14]. Myopathy is a disease related to muscles [15], whereas neuropathy is a neuromuscular disease that disturbs the normal functioning of the nerves in the body. The nerves that control voluntary muscles are affected by the neuromuscular disorders and symptoms may include muscle rigidity and weakness, muscle pain and loss of muscular control. Nerves work like wires that carry signal from the brain to the body and return back from the body to the brain. When the normal operation of the nerves is disturbed, the condition is called neuropathy [16]. It's difficult and may be inaccurate to diagnose neuromuscular disorders by visual inspection of EMG signals. The development of automated systems that help to diagnose neuromuscular disorders will be allowed by collecting the data of EMG signals [17]. A system is therefore proposed that will automatically classify the anomalies of the hamstring and quadriceps muscles involved in knee joint movements.

For the detection of anomalies in muscle activities multiple signal classification techniques have been suggested in [18], [19]. Pattern classification-based control systems extract a set of time, frequency and time-frequency domain features that describe the sEMG signals in order to recognize various forms of motion. Extracted features from sEMG data have been used to classify the sEMG signals [20]–[22]. Classification accuracies greater than 90 percent have been reported in [23], [24]. A comparison study has been done in [25], [26], concluded that the selection of features impacts significantly on the performance of classification than the selection of classifiers. Due to the technological advancements in computer hardware and software, the processing of complex machine learning algorithms on huge datasets becomes fast and easy. From the sEMG signal which changes as a function of time, features can be calculated in the form of numeric values.

Time-domain features have been vastly used in sEMG signal classification because they are very simple to calculate, easy to apply and no signal transformation is required. Hudgins uses four time-domain features for the classification of the sEMG signals, more commonly known as Hudgins Time-Domain Features [27]. Increasing the number of time domain features can drastically increase the classification accuracy of the same classification algorithm without the need to increase the processing power [28]. In this study, Enhanced Wavelength (EWL), Log Detector (LD), Mean Absolute Value (MAV), Maximum Fractal Length (MFL), Difference Absolute Standard Deviation Value (DASDV), Modified Mean Absolute Value (MMAV), Average Amplitude Change (AAC), Simple Square Integral (SSI), Enhanced Mean absolute value (EMAV), Waveform Length (WL), Standard Deviation (STD), Root Mean Square (RMS), Integrated EMG (IEMG) and Variance

(VAR) have been used as input features for Support Vector Machine (SVM) algorithm for the classification of sEMG signals. During the study, flexion and extension of three kinds of exercises were selected for the movement of the knee joint. In inclusion, four muscles (two from hamstring and two from quadriceps) which are involved in knee joint motion were selected for acquiring the sEMG data.

The working has been comprised of four stages:

- Data acquisition
- Feature extraction
- Classification of abnormalities using SVM and cross-validation using k-fold
- App designing.

2. Materials and Methods

While comparative analysis it was observed that the previous studies focused on the classification of the abnormalities and myopathies using sEMG signal but their main focus was on upper-limb muscles [9]–[13]. They also prefer to use neural networks for classification purposes, therefore, we focused on the lower limbs and also used the classical machine learning algorithm SVM, which takes less computational power as compared to the complex algorithms of deep learning. The system is proposed to recognize and classify the abnormalities involved in the lower-limb muscles recorded from four sEMG channels by using DFRobot's EMG sensors and SVM algorithm, and to evaluate the classification accuracy of recorded sEMG signals using k-fold crossvalidation method.

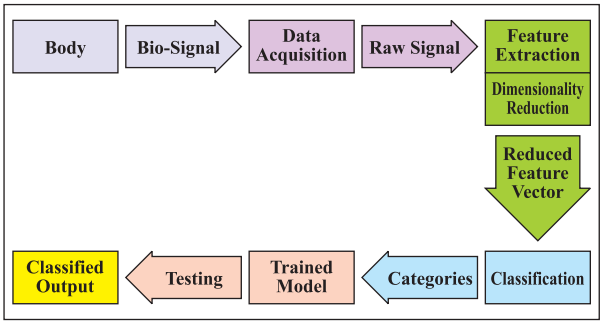

Fig 1. Block diagram of the proposed system.

The block diagram of the proposed methodology is shown in Fig 1, which comprises of placement of sensors on the hamstring (semitendinosus, biceps femoris) and quadriceps (vastus medialis, rectus femoris) muscles for the detection classifier is trained by using the reduced feature vectors in order to classify the healthy and unhealthy muscles. The classification accuracy for recognition of healthy and unhealthy muscles of the trained model is verified by using the k-fold cross-validation technique (where k=5). The whole process is repeated three times for the three exercises, given in Table 1.

Table 1. Exercises Performed

Exercises	Details	ROM
Lying-Down	5 Times (Flexion & Extension)	0° to 140°
Walking	5 Strides (10 Steps)	0° to 60°
Sitting	5 Times (Flexion & Extension)	90° to 130°

2.1 Subject and Data Acquisition

The sEMG signal was acquired from the hamstring and quadriceps muscles using four Gravity Analog EMG Sensors made by OYMotion and DFRobot. Each sensor consists of a signal transmitter board and a dry electrode board connected through a singledifferential probe. To acquire noiseless sEMG, the sEMG sensors should have a high signal to noise ratio and a high common-mode rejection ratio [29]. The sensor contains a builtin amplifier circuit and filtering circuit that amplify the signals (1000 times within ±1.5mV) and reduces noises (baseline noise and power line interference frequency) respectively. As the EMG signal is different in different positions, even on the same person so to ensure that the signal is free of distortion and noise, each sensor is calibrated before every use. Subject was asked to calm down and relax for a while to check the waveform on the Arduino's serial monitor. If the wave is forming (before calibration), as shown in Fig 2, then the position of the dry electrode is fine-tuned (calibrated), such that there is no distortion left and the waveform becomes a straight line at 0, as shown in Fig 3. The units in the Fig 2 and Fig 3 are; time (in millisecond) on x-axis and amplitude (in microvolt) on y-axis.

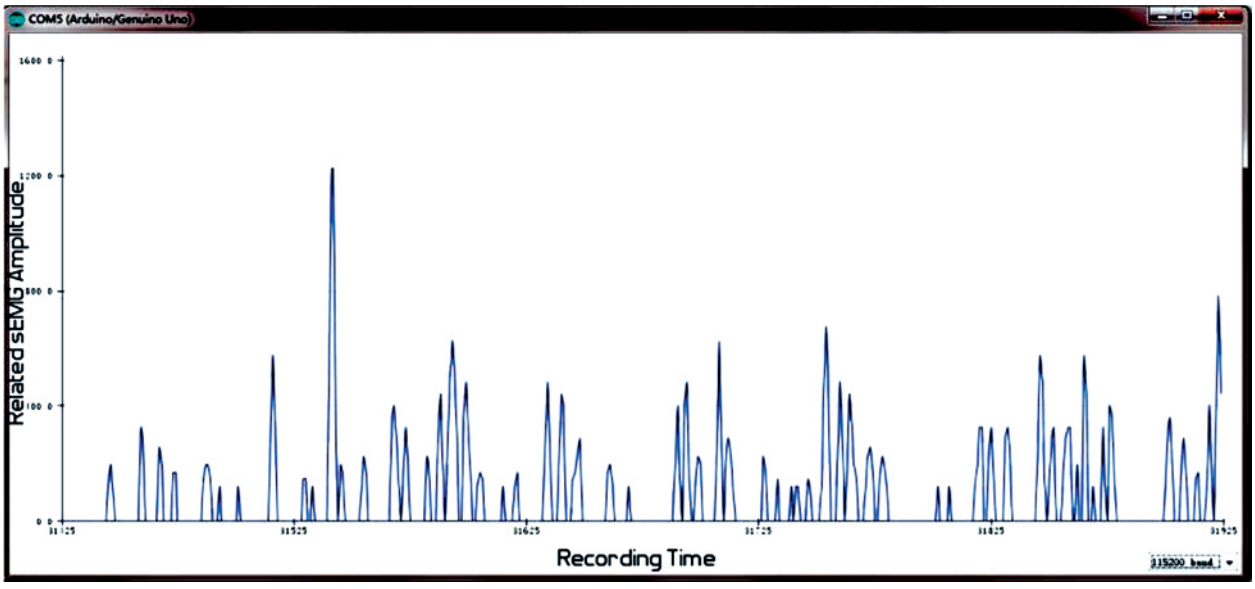

Fig 2. Before calibration of the EMG sensors.

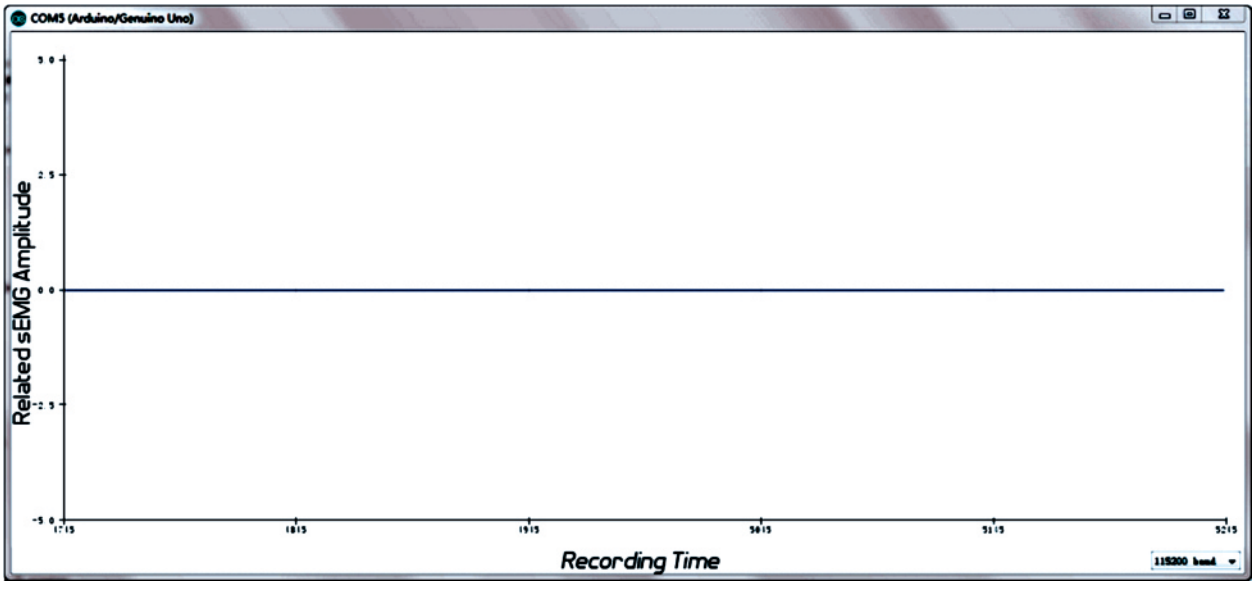

Fig 3. After calibration of the EMG sensors.

The range of output voltage varies from 0 to 3V having the reference voltage 1.5V. The supplied current should be at least 20mA while the supplied voltage varies from 3.3 to 5.5V. The range of the operative spectrum varies from 20Hz to 500Hz. Placing the dry electrode board should be consistent with the muscle's direction. The signal of each muscle is then sampled at 1KHz and digitally converted using Arduino UNO, which has a built-in 10 bit A/D converter. Due to the use of electrode board (Plate Size: 22mm * 35mm with short inter-electrode distance 5mm), no problem of crosstalk was detected. The system block diagram including MyoGenu Box, EMG sensors, probes, microcontroller is as depicted in Fig 4.

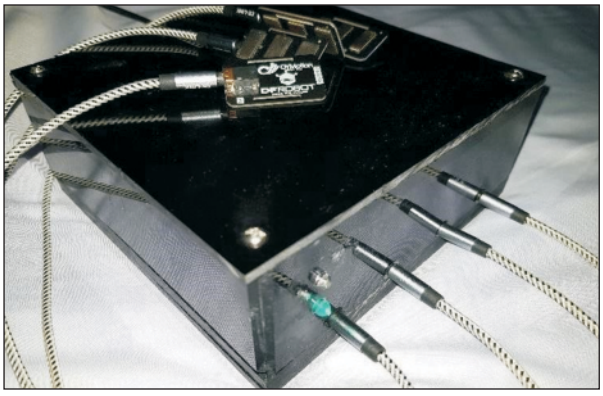

Fig 4. A Fig of the entire system (MyoGenu Box)

We made sure that all the subjects were given rest for a few minutes so that their muscles could relax which eliminated the possibility of muscle fatigue. The moisture content can weaken the signal [30], so there should not be any sweat drops on the skin. The mean temperature during the procedure was between 25° Celsius to 35° Celsius.

The placement of sensors was identified under the supervision of senior Doctor, Department of Physiotherapy, Dr. Ziauddin Hospital (Karachi, Pakistan). Electrodes were positioned according to Winter's guidelines [31]. All the subjects signed informed consent forms before performing the experiments. Subject's personal data were treated according to the Personal Data Protection Bill 2018.

During the experiment, the sensors were attached on the right thigh of the subject and it was made sure that the signals were normal according to the signal check procedures [32]. The two sensors were placed on the hamstring (semitendinosus, biceps femoris) muscles and the other two sensors were placed on the quadriceps (vastus medialis, rectus femoris) muscles, as shown in Fig 5.

The model needs to be trained so that it can classify between healthy and unhealthy muscles. For this purpose, the study was conducted on a total of 151 subjects (all males). Among them 140 subjects were healthy and 11 subjects were unhealthy. Data were recorded from 140 healthy subjects (all males) with ages ranging from 18 to 30 years (age 24.0 ± 3.7 years; height 175 ± 7.4 cm; mass 70 ± 11.3 kg; BMI-range 15–33.5 kg/m²). Exclusion criteria involve a history of neurological diseases related to the knee, osteoporosis, osteoarthritis, knee injuries, orthopedic surgery, and an irregular gait. The data of 11 unhealthy subjects (all males) was acquired from the online machine learning repository UCI [33], with some abnormality in the knee previously diagnosed, including disorders and injuries related to knee and/or having a problem in their walking pattern.

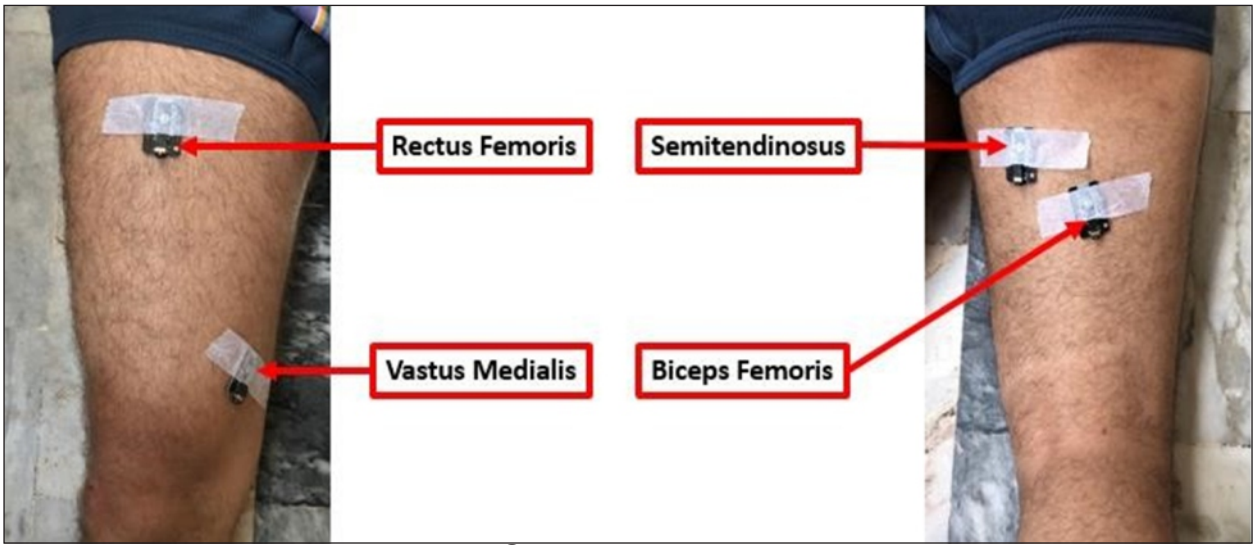

2.2 Feature Extraction

Feature extraction is a computational method used to acquire the necessary information from various signals by applying different formulae. Since the time-domain features are based on signal amplitude and do not need a transformation, thus mostly used for myoelectric classification [27]. A powerful system for classification include; data acquisition, filtration, feature extraction, feature reduction and finally data classification. The sEMG signal's frequency is 10–1000Hz, and most of the signal is concentrated in the range of 50–150Hz [34]. The acquired data is then filtered through a bandpass filter of the range 50.1-150Hz with a sampling frequency of 1000Hz and the signal is then passed through a bandstop filter as well of the range 49.9-50.1Hz to remove the line frequency (noise) of 50Hz. A new feature set is introduced that helps to acquire the useful pieces of information from sEMG data for the classification of normal and abnormal muscle's data.

The Time-Domain features used are given as:

2.2.1 Average Amplitude Change (AAC)

Change in a signal can be calculated by using Average Amplitude Change, given as

$$AAC = \frac{1}{N}\sum_{i=1}^{N-1} |xi + 1 - xi|^2 \quad (1)$$

where 'N' is the total number of samples and 'Xi' is data.

2.2.2 Log Detector (LD)

Calculates the strength of the signal obtained during the contraction of muscle that changes as the signal amplitude changes, given as

$$LD = \exp\exp\left(\frac{1}{N}\sum_{i=1}^{N} log(|x_i|)\right) \quad (2)$$

2.2.3 Mean Absolute Value (MAV)

Estimates the average of the absolute values of a given signal _x', given as

$$MAV = \frac{1}{L}\sum_{k=1}^{L} |x_k| \quad (3)$$

where 'xk' is the kth sample in the given signal.

2.2.4 Maximum Fractal Length (MFL)

Measures sEMG signal patterns at low-level muscle contraction, given as

$$MFL = log_{10}\left(\sum_{i=1}^{L-1} |x_{i+1} - x_i|\right) \quad (4)$$

2.2.5 Simple Square Integral (SSI)

It is calculated using the sEMG signal energy, given as

$$SSI = \sum_{i=1}^{N} (|x_i^2|) \quad (5)$$

2.2.6 Waveform Length (WL)

Describes the complexity of the waveform by calculating the cumulative length of the waveform over the segment, given as

$$WL = \sum_{k=1}^{L} |\Delta x_k| \quad (6)$$

where,

$$\Delta x_k = x_k - x_{k-1}$$

2.2.7 Integrated EMG (IEMG)

It is defined as, the summation of the absolute values of sEMG signals that can be treated as a signal power estimator, given as

$$IEMG = \sum_{i=1}^{N} |x_i| \quad (7)$$

2.2.8 Root Mean Square (RMS)

RMS is the under root of the mean of the square of the vertical distance, given as

$$RMS = \sqrt{\frac{1}{N}\sum_{i=1}^{N} {x_i}^2} \quad (8)$$

2.2.9 Standard Deviation (STD)

It measures how much the data differ from the mean and is used in comparison to the mean, given as

$$STD = \sqrt{\frac{\sum_{i=1}^{N} (x_i - \underline{x})^2}{N-1}} \quad (9)$$

where $\underline{x}$ represents the mean value.

2.2.10 Variance (VAR)

It measures the power of the signal, given as

$$VAR = \frac{1}{N-1} \sum_{i=1}^{N} {x_i}^2 \quad (10)$$

2.3 Classification

In the present work, we used the cubic SVM classifier for the classification of healthy and unhealthy sEMG signals obtained from the hamstring and quadriceps muscles, involved in knee joint motion. SVM is extremely recommended by many [35], [36] as it is an efficient and effective machine learning algorithm that gives substantial accuracy with minimal computational power. The fundamental principle of the SVM is to find an optimum separation hyperplane with the maximum distance between the support vectors of two classes [16], [37], [38].

As there are two classes healthy and unhealthy, it means it is a binary classification task, therefore SVM classifier is chosen. Three types of kernel functions were used for the classification of sEMG data. The results of different kernel functions were compared by calculating their classification accuracies. The results show that the cubic kernel function was best amongst all. The typical confusion matrix and the parameters acquired from it are shown in Table 2.

Table 2. A Typical Confusion Matrix

	Predicted Class	
True Class	True Positive (TP)	False Negative (FN)
	False Positive (FP)	True Negative (TN)

In Table 2, TP, TN, FP, and FN are given. The parameters that can be calculated from a confusion matrix are given below:

2.3.1 True Positive

When the positive is classified as positive.

2.3.2 False Negative

When the positive is classified as negative.

2.3.3 True Negative

When the negative is classified as negative.

2.3.4 False Positive

When the negative is classified as positive.

2.4 App Designing

An app named "MyoGenu App" was also designed to assist the user by providing an easy to use Graphical User Interface (GUI). The MyoGenu App has two stages, training and testing, as shown in Fig 6 and Fig 7, which was built by using the MATLAB R2019b [39]. When the user opens the app training screen of the app will display the classification accuracies on the screen for each of the twelve models. On the right side of the app, when the user clicks the testing button the app will ask for the sEMG data of the new subject and predict it to classify each of the four muscles as normal or abnormal and give the output on the screen.

Fig 6. The training window of the MyoGenu App

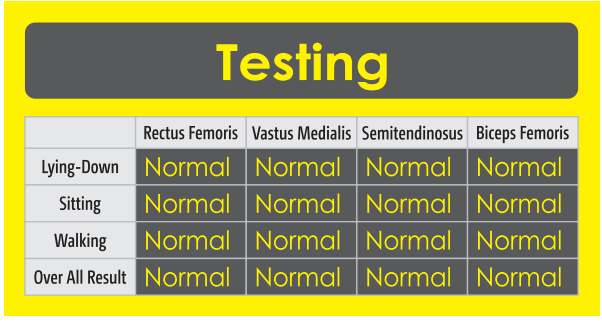

Fig 7. The testing window of the MyoGenu App

3. Results and Discussion

The results are shown in a confusion matrix, separately for each of the four muscles involved in each of the three exercises. Three exercises are recorded, as shown in Table I, to acquire the raw sEMG data, which is then filtered to eliminate the noise using the bandpass filter of range 50.1-150Hz and bandstop filter of range 49.9-50.1Hz, and finally features are extracted for the classification.

The classification tasks are performed by using an algorithm SVM. It is a classifier that separates the different classes by constructing hyperplanes. The data of each sample are so mapped that the healthy and unhealthy classes are separated by a clear and widest possible boundary. The validation is done using a k-fold cross-validation technique (where k=5) for training each of the twelve models (4 muscles × 3 exercises).

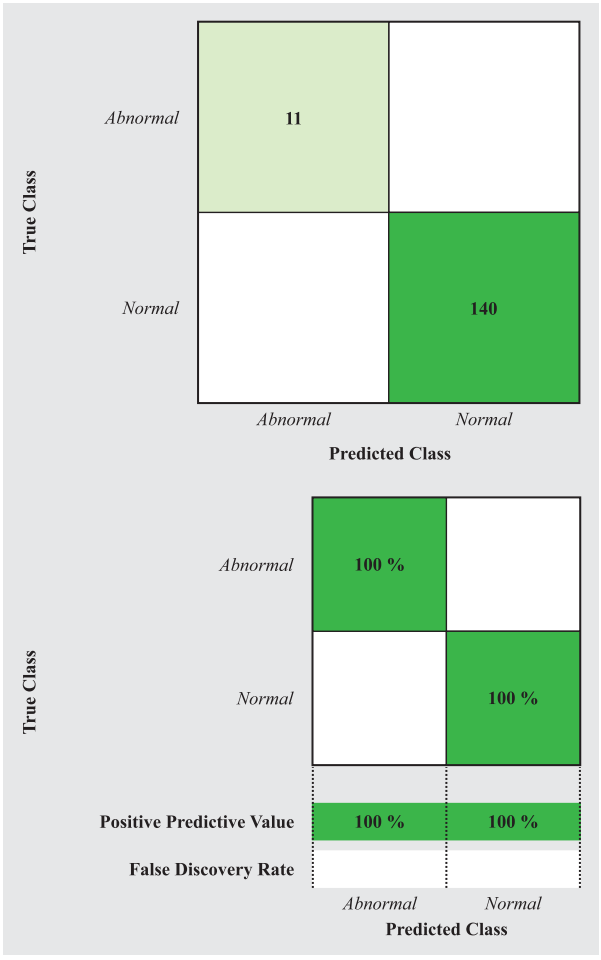

Fig 8. Confusion matrix of rectus femoris while lying down

The SVM algorithm is implemented using the classification learner app of MATLAB R2019b. While testing, 11 out of 12 models predicted all the 11 samples of 'abnormal' class as abnormal while all the 140 samples of 'normal' class as normal. The model predicted all the samples correctly, thus the Positive Predictive Value (PPV) for both the 'normal' and 'abnormal' class is 100% which makes the False Discovery Rate (FDR) for both the classes as 0%, as shown in Fig 8 to Fig 10 and Fig 12 to Fig 19. While testing the 12th model, predicted 150 samples correctly out of a total of 151 samples for biceps femoris muscle while performing the flexion and extension of the knee joint at the lying down

position. The model predicted one sample of 'normal' class as abnormal, thus the PPV of the abnormal class is 92%, whereas the FDR of 'abnormal' class is 8%. None of the 'abnormal' class's sample is predicted as normal, thus the PPV of the 'normal' class is 100% which makes FDR of the 'normal' class as 0%, as shown in Fig 11. For the future researchers it is recommended that, instead of downloading the data of unhealthy subjects from the internet, focus on acquiring it by yourself.

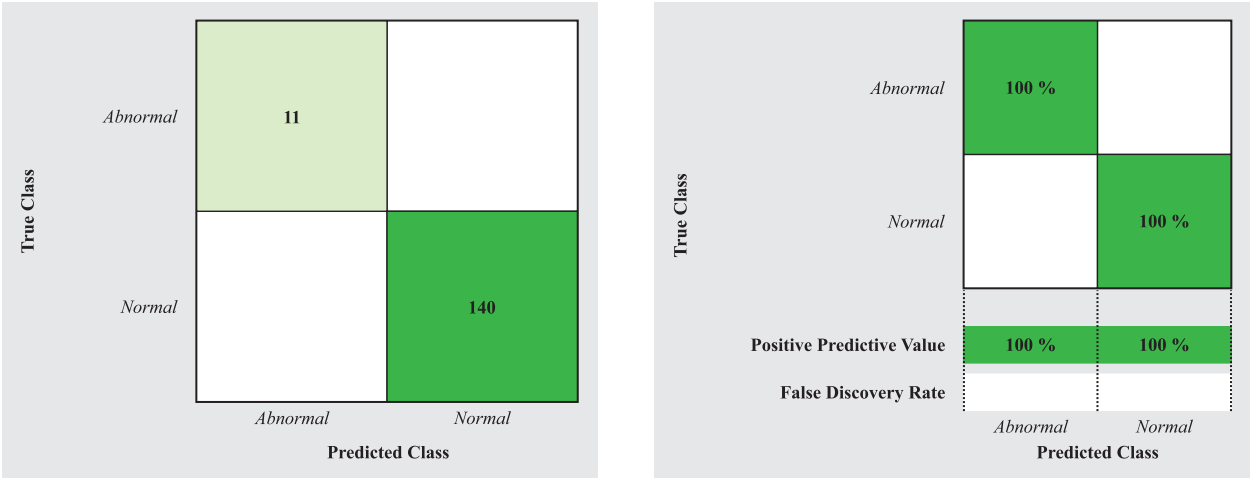

Fig 9. Confusion matrix of vastus medialis while lying down

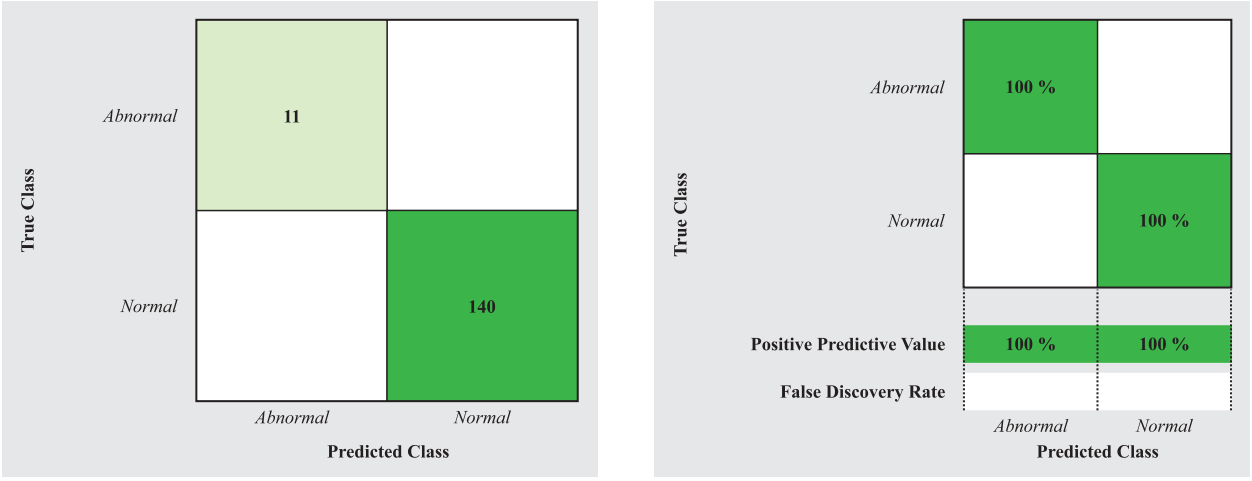

Fig 10. Confusion matrix of semitendinosus while lying down

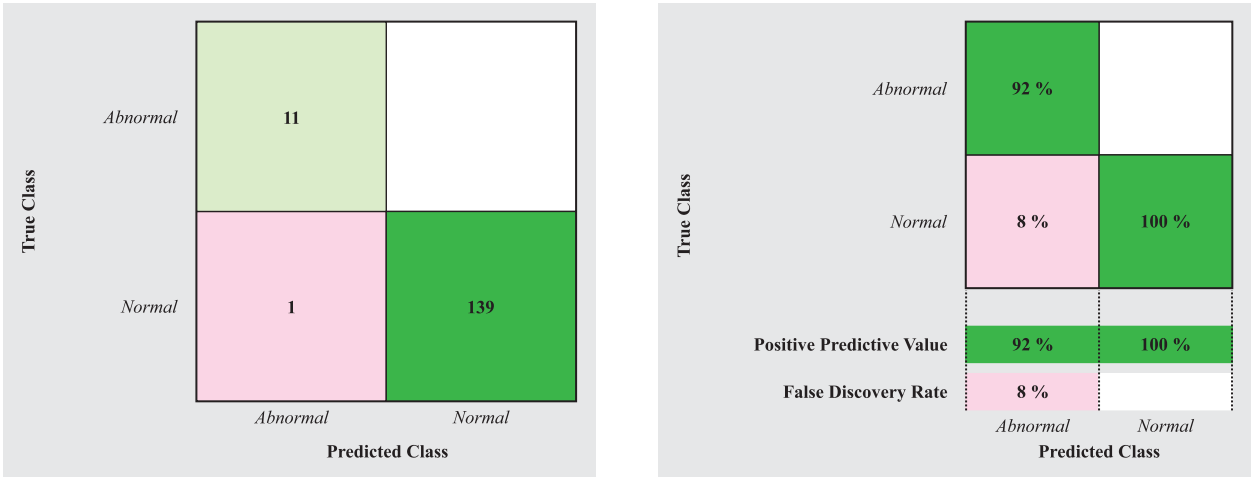

Fig 11. Confusion matrix of biceps femoris while lying down

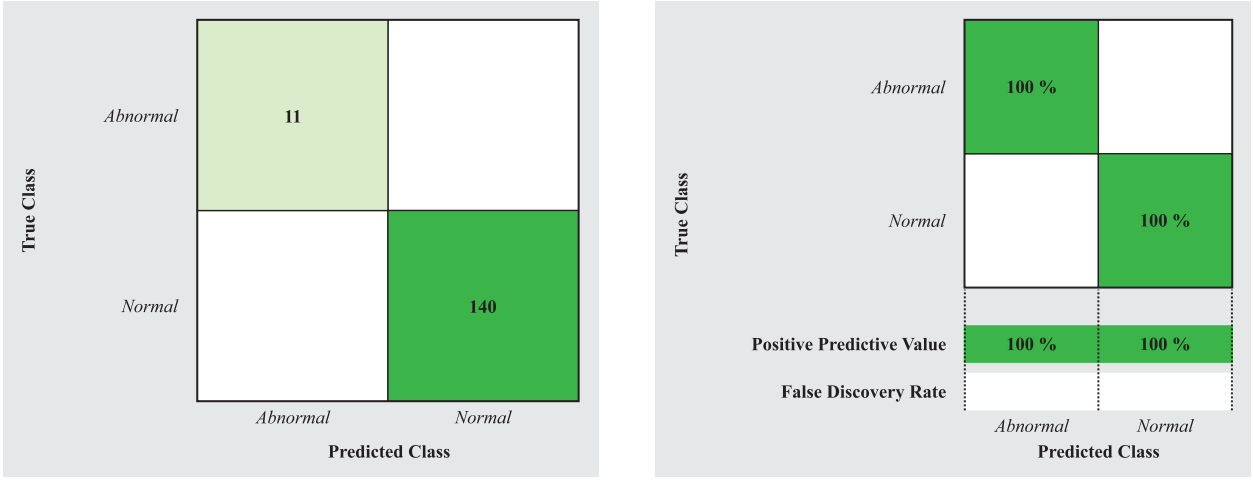

Fig 12. Confusion matrix of rectus femoris while sitting

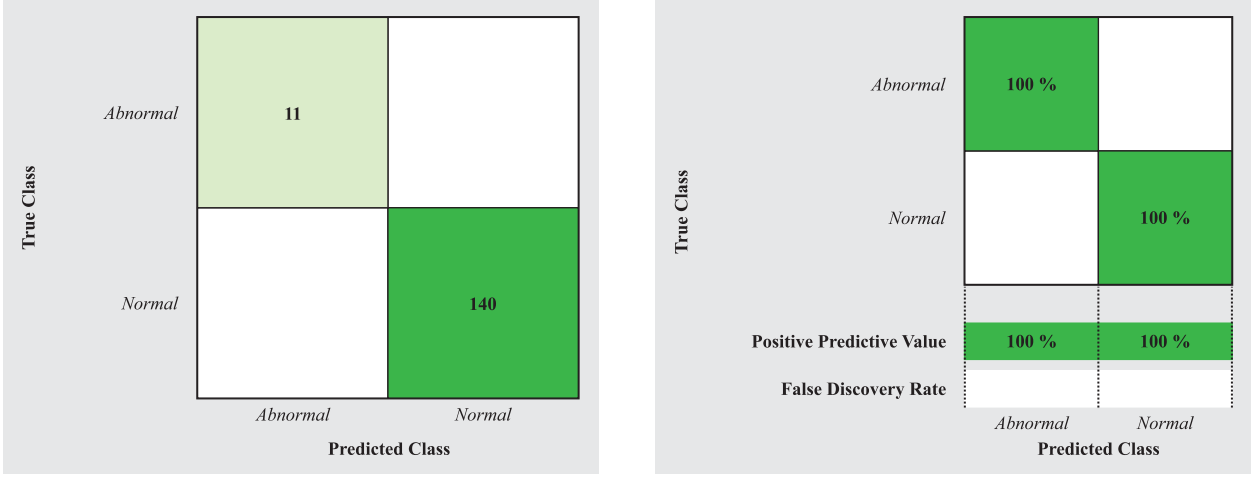

Fig 13. Confusion matrix of vastus medialis while sitting

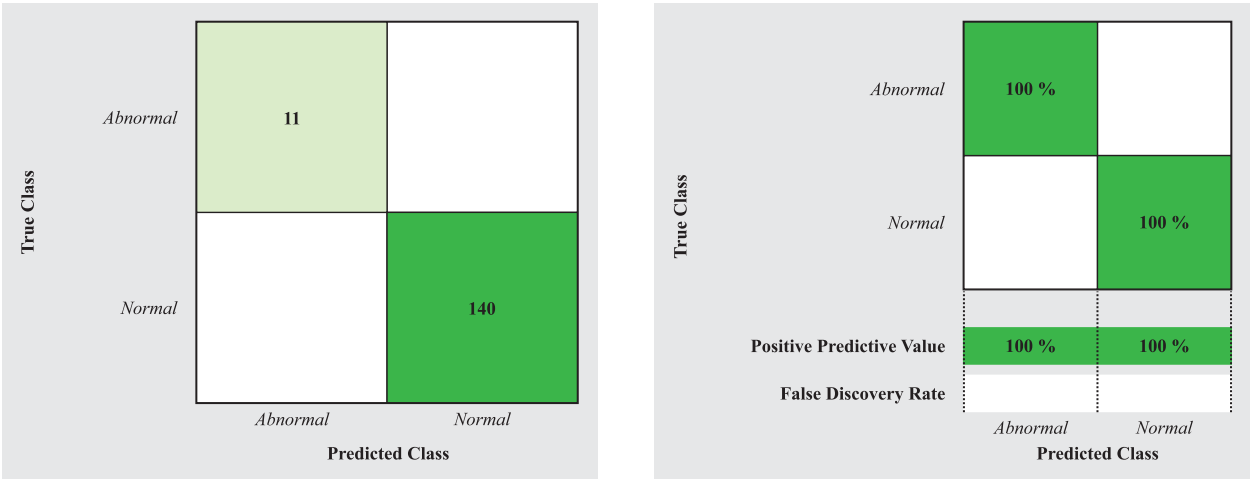

Fig 14. Confusion matrix of semitendinosus while sitting

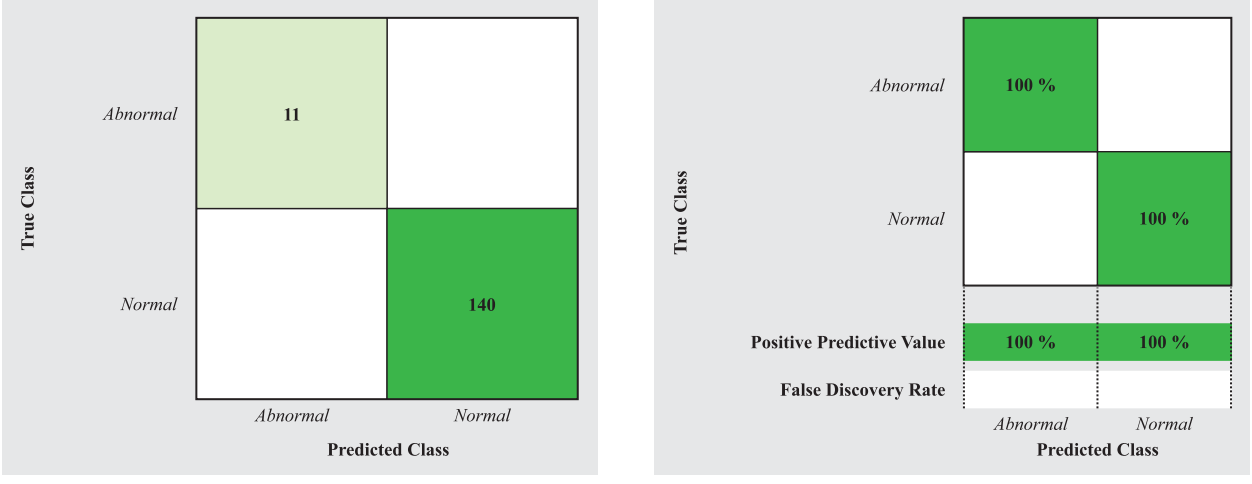

Fig 15. Confusion matrix of biceps femoris while sitting

Fig 16. Confusion matrix of rectus femoris while walking

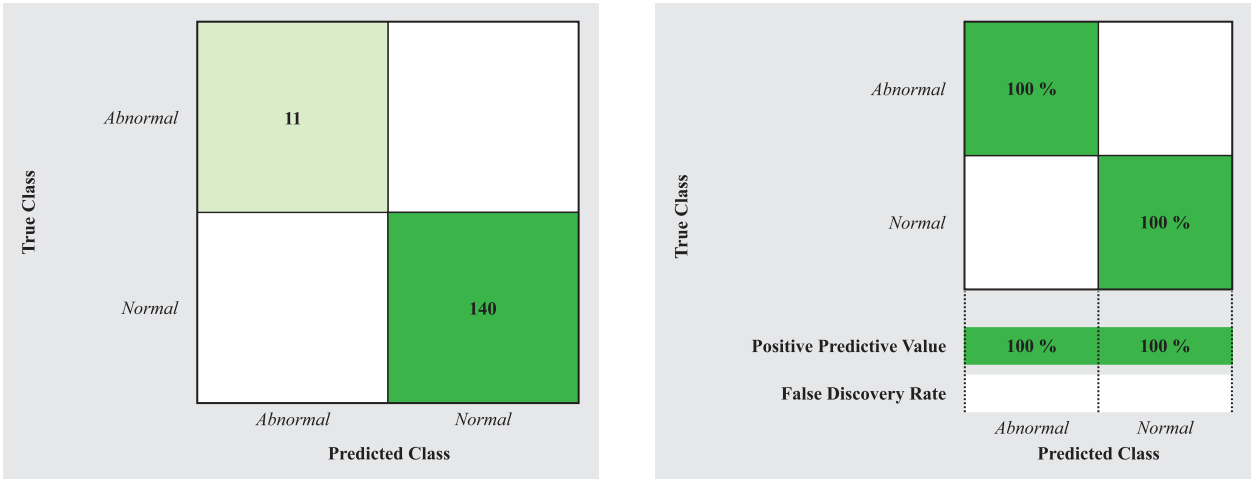

Fig 17. Confusion matrix of vastus medialis while walk

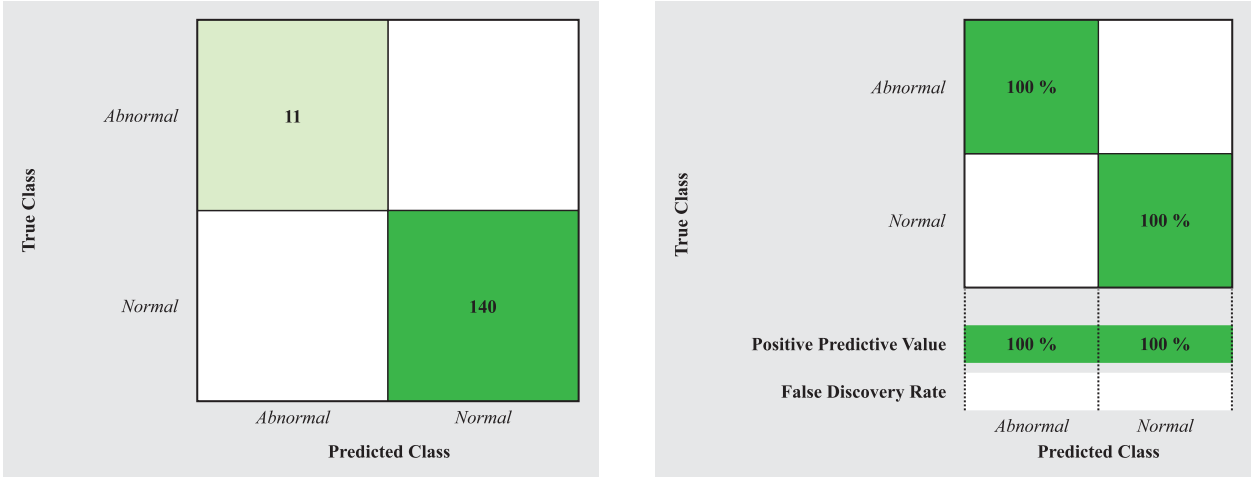

Fig 18. Confusion matrix of semitendinosus while walking

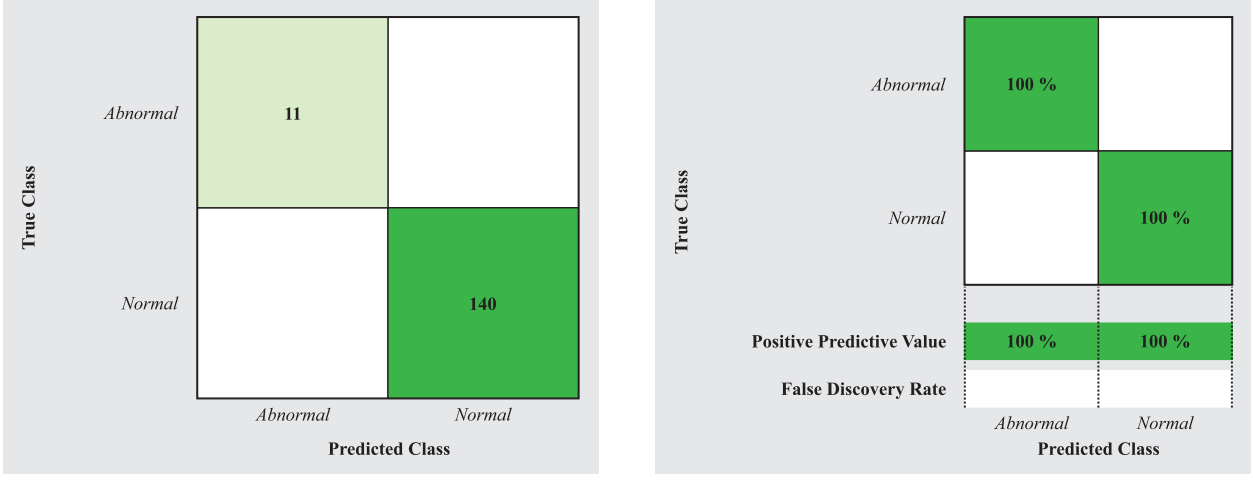

Fig 19. Confusion matrix of biceps femoris while walking

3.1 Positive Predictive Value

The positive predictive value is given as

$$PPV = \frac{No.\ of\ TP}{No.\ of\ TP + No.\ of\ FP} \quad (11)$$

3.2 False Discovery Rate

The false discovery rate (FDR) is given as

$$FDR = \frac{No.\ of\ FP}{No.\ of\ FP + No.\ of\ TP} \quad (12)$$

4. Conclusion

The study has been focused on the classification of sEMG signals of healthy and unhealthy muscles which are involved in knee joint motion using Arduino [40] and DFRobot's EMG sensors [41]. Computational techniques were applied for extracting ten time-domain features. The obtained feature vectors were then sent to the SVM classifier to train the model. It has been observed that the proposed model trained on the given features has delivered significantly better performance, and is reliable and fast compared to other existing classifying techniques. The validation was done by using a k-fold cross validation technique, giving the classification accuracy of 99%. Therefore, the proposed automatic classification system can be used for automated detection and classification of anomalies in the knee muscles.

References

[1] W. M. B. Wan Daud, A. Yahya, S.-H. Chong, M. F. Sulaima, and R. Sudirman, "Features Extraction of Electromyography Signals in Time Domain on Biceps Brachii Muscle," International Journal of Modeling and Optimization, vol. 3, pp. 515-519, Dec. 2013.

[2] M. B. I. Raez, M. S. Hussain, and F. Mohd-Yasin, "Techniques of EMG signal analysis: detection, processing, classification and applications," Biol Proced Online, vol. 8, pp. 11-35, Mar. 2006.

[3] K. Kiguchi, Y. Imada, and M. Liyanage, "EMG-Based Neuro-Fuzzy Control of a 4DOF Upper-Limb Power-Assist Exoskeleton," in 2007 29th Annual International Conference of the IEEE Engineering in Medicine and Biology Society, 2007, pp. 3040-3043.

[4] L. Dipietro, M. Ferraro, J. J. Palazzolo, H. I. Krebs, B. T. Volpe, and N. Hogan, "Customized interactive robotic treatment for stroke: EMG-triggered therapy," IEEE Transactions on Neural Systems and Rehabilitation Engineering, vol. 13, no. 3, pp. 325-334, Sep. 2005.

[5] C. Choi, S. Micera, J. Carpaneto, and J. Kim, "Development and Quantitative Performance Evaluation of a Noninvasive EMG Computer Interface," IEEE Transactions on Biomedical Engineering, vol. 56, no. 1, pp. 188-191, Jan. 2009.

[6] "Muscles Alive-their functions revealed by electromyography," Postgrad Med J, vol. 39, no. 449, p. 162, Mar. 1963.

[7] T. A. Kuiken et al., "Targeted Muscle Reinnervation for Real-time Myoelectric Control of Multifunction Artificial Arms," JAMA, vol. 301, no. 6, pp. 619-628, Feb. 2009.

[8] Y. C. Jo, H. Na Kim, W. H. Hwang, H. Ki Hong, Y. S. Choi, and S. Won Jung, "Wearable Patch Device for Uterine EMG and Preterm Birth Monitoring Applications," in TENCON 2018 - 2018 IEEE Region 10 Conference, 2018, pp. 1127-1130.

[9] A. Zhang, N. Gao, L. Wang, and Q. Li, "Combined Influence of Classifiers, Window Lengths and Number of Channels on EMG Pattern Recognition for Upper Limb Movement Classification," in 2018 11th International Congress on Image and Signal Processing, BioMedical Engineering and Informatics (CISP-BMEI), 2018, pp. 1-5.

[10] M. S. Çelik and Eminolu, "Fuzzy logic based classification for multifunctional upper limb prostheses," in 2016 Medical Technologies National Congress (TIPTEKNO), 2016, pp. 1-4.

[11] O. W. Samuel et al., "Intelligent EMG Pattern Recognition Control Method for Upper-Limb Multifunctional Prostheses: Advances, Current Challenges, and Future Prospects," IEEE Access, vol. 7, pp. 10150-10165, 2019.

[12] O. W. Samuel, X. Li, P. Fang, and G. Li, "Examining the effect of subjects' mobility on upper-limb motion identification based on EMG-pattern recognition," in 2016 Asia-Pacific Conference on Intelligent Robot Systems (ACIRS), 2016, pp. 137-141.

[13] S. Pancholi and A. M. Joshi, "Time Derivative Moments Based Feature Extraction Approach for Recognition of Upper Limb Motions Using EMG," IEEE Sensors Letters, vol. 3, no. 4, pp. 1-4, Apr. 2019.

[14] P. Aagaard, E. B. Simonsen, J. L. Andersen, S. P. Magnusson, F. Bojsen Møller, and P. Dyhre Poulsen, "Antagonist muscle coactivation during isokinetic knee extension," Scandinavian Journal of Medicine & Science in Sports, vol. 10, no. 2, pp. 58-67, 2000.

[15] N. S. Anand and D. Chad, "Electrophysiology of Myopathy," in The Clinical Neurophysiology Primer, A. S. Blum and S. B. Rutkove, Eds. Totowa, NJ: Humana Press, 2007, pp. 325-351.

[16] S. S. Roy et al., "Detection of Healthy and Neuropathy Electromyograms Employing Stockwell Transform," in 2018 IEEE Applied Signal Processing Conference (ASPCON), 2018, pp. 214-218.

[17] V. Bajaj and A. Kumar, "Features based on intrinsic mode functions for classification of EMG signals," International Journal of Biomedical Engineering and Technology, vol. 18, pp. 156-167, Jun. 2015.

[18] J. Lee, Y. Kagamihara, and S. Kakei, "Quantitative evaluation of cerebellar ataxia based on pathological patterns of the muscle activities," in 2013 35th Annual International Conference of the IEEE Engineering in Medicine and Biology Society (EMBC), 2013, pp. 902-905.

[19] L.-G. Zhang and R. Shiavi, "EMG pattern classification of normal and anterior cruciate ligament injured subjects," in Proceedings of the Annual International Conference of the IEEE Engineering in Medicine and Biology Society, 1988, pp. 1192-1193 vol.3.

[20] A. Phinyomark, G. Chujit, P. Phukpattaranont, C. Limsakul, and Huosheng Hu, "A preliminary study assessing time-domain EMG features of classifying exercises in preventing falls in the elderly," in 2012 9th International Conference on Electrical Engineering / Electronics, Computer, Telecommunications and Information Technology, 2012, pp. 1-4.

[21] E. N. Kamavuako, E. J. Scheme, and K. B. Englehart, "Combined surface and intramuscular EMG for improved real-time myoelectric control performance," Biomedical Signal Processing and Control, vol. 10, pp. 102-107, Mar. 2014.

[22] A. Phinyomark, F. Quaine, S. Charbonnier, C. Serviere, F. Tarpin-Bernard, and Y. Laurillau, "EMG feature evaluation for improving myoelectric pattern recognition robustness," Expert Systems with Applications, vol. 40, no. 12, pp. 4832-4840, Sep. 2013.

[23] M. A. Oskoei and H. Hu, "Support Vector Machine-Based Classification Scheme for Myoelectric Control Applied to Upper Limb," IEEE Transactions on Biomedical Engineering, vol. 55, no. 8, pp. 1956-1965, Aug. 2008.

[24] K. Englehart, B. Hudgins, P. A. Parker, and M. Stevenson, "Classification of the myoelectric signal using time-frequency based representations," Medical Engineering & Physics, vol. 21, no. 6, pp. 431-438, Jul. 1999.

[25] L. J. Hargrove, K. Englehart, and B. Hudgins, "A Comparison of Surface and Intramuscular Myoelectric Signal Classification," IEEE Transactions on Biomedical Engineering, vol. 54, no. 5, pp. 847-853, May 2007.

[26] Z. Arief, I. A. Sulistijono, and R. A. Ardiansyah, "Comparison of five time series EMG features extractions using Myo Armband," in 2015 International Electronics Symposium (IES), 2015, pp. 11-14.

[27] B. Hudgins, P. Parker, and R. N. Scott, "A new strategy for multifunction myoelectric control," IEEE Trans Biomed Eng, vol. 40, no. 1, pp. 82-94, Jan. 1993.

[28] M. Zardoshti-Kermani, B. C. Wheeler, K. Badie, and R. M. Hashemi, "EMG feature evaluation for movement control of upper extremity prostheses," IEEE Transactions on Rehabilitation Engineering, vol. 3, no. 4, pp. 324-333, Dec. 1995.

[29] Y. Zhou, Y. Fang, K. Gui, K. Li, D. Zhang, and H. Liu, "sEMG Bias-Driven Functional Electrical Stimulation System for Upper-Limb Stroke Rehabilitation," IEEE Sensors Journal, vol. 18, no. 16, pp. 6812-6821, Aug. 2018.

[30] S. Pancholi and A. M. Joshi, "Portable EMG Data Acquisition Module for Upper Limb Prosthesis Application," IEEE Sensors Journal, vol. 18, no. 8, pp. 3436-3443, Apr. 2018.

[31] D. A. Winter, Biomechanics and Motor Control of Human Movement. John Wiley & Sons, 2009.

[32] P. Konrad, The ABC of EMG: a practical introduction to kinesiological electromyography, Version 1.4. Noraxon USA, Inc, 2006.

[33] https://archive.ics.uci.edu/ml/datasets/EMG+dataset+in+Lower+Limb.

[34] A. Qingsong, Q. Liu, and W. Meng, "Neuromuscular Signal Acquisition and Processing," 2018, pp. 33-66.

[35] L. R. Quitadamo et al., "Support vector machines to detect physiological patterns for EEG and EMG-based human-computer interaction: a review," J. Neural Eng., vol. 14, no. 1, p. 011001, Jan. 2017.

[36] T. Lorrain, N. Jiang, and D. Farina, "Surface EMG classification during dynamic contractions for multifunction transradial prostheses," Conf Proc IEEE Eng Med Biol Soc, vol. 2010, pp. 2766-2769, 2010.

[37] S. Badani, S. Saha, A. Kumar, S. Chatterjee, and R. Bose, "Detection of epilepsy based on discrete wavelet transform and Teager-Kaiser energy operator," in 2017 IEEE Calcutta Conference (CALCON), 2017, pp. 164-167.

[38] S. Chatterjee, S. Pratiher, and R. Bose, "Multifractal detrended fluctuation analysis.

[39] Based novel feature extraction technique for automated detection of focal and nonfocal electroencephalogram signals," IET Science, Measurement & Technology, vol. 11, no. 8, pp. 1014-1021, Jul. 2017.

[40] mathworks.com/products/new_products/release2019b.html?requestedDomain=

[41] https://www.arduino.cc/

[42] https://www.dfrobot.com/product-1661.html

ISSN NO. 2706-9648

Pakistan Journal of Engineering

For online access, please visit:
journal.pec.org.pk

DESIGN OF PATTERN RECONFIGURABLE ANTENNA ARRAY

Muhammad Amir, Muhammad Farooq, Salman Illahi, Jehan Dastagir, Shahid Bashir

ARTICLE INFO

Article History:

Accepted 16 Oct 2020

Published on 25 Oct 2020

Keywords

CST, Antenna, Diode, Gain, Directivity.

ABSTRACT

Static antennas with beam steering for controlled area coverage are need of the day. This paper presents a two element radiation pattern reconfigurable antenna array having a delayed line feeding technique. The proposed antenna is designed for working in 2.4GHz band having three different radiation patterns. In the proposed design, six PIN diode switches in separate configurations are used for changing the direction of the main radiation beam. Such different combinations of switches produce different radiation patterns exhibiting improved bandwidths, directivities and gain at each condition.

1. Introduction

Antenna is an important part of wireless communication whose presence is compulsory in order to transmit and receive signals without wires [1]. Every antenna has unique properties such as resonance frequency, particular polarization and radiation pattern. Usually, all above mentioned properties are fixed for an ordinary antenna. Nowadays, frequency reconfigurable [2,3], polarization reconfigurable [4,5] and radiation pattern reconfigurable antennas [6,7] are taking interest of many researchers. Normally, the radiation direction of the main beam of antenna can be changed by manually or mechanically moving around the antenna. On the other hand, it is much interesting to change the direction of the main beam without moving the antenna but by merely using some switches. This concept increases the coverage area of an antenna thus the need for installing numerous antennas for maximum coverage is no longer present. Such a design will remove the need for mechanically moving antenna arrays again and again [8]. There are a number of methods for making radiation pattern reconfigurable. In scheme, two patches are placed at +45°and -45° along with a switch to ON and OFF each patch alternately and get radiation patterns at +30°and -30° [9].

Using an array of numerous patches is also an efficient way of designing a pattern reconfigurable antenna as it increases the degree of freedom. For this, a 2 x 2 array is used with feeding delay line having a complex design but operates at 7.5GHz with three different radiation patterns i.e. at +30°, 0°and -30° [10]. In this array, the authors used switches and with different combination of these switches, the stated radiation patterns were

achieved. In a single element radiation pattern, reconfigurable antenna is introduced using different switches to change the direction of the main beam from antenna [11,12,13].

Here, in this paper, PIN diodes are used which are very useful for designing of any type of reconfigurable antennas. PIN diodes can be switched ON or OFF, in each case it has a different representation [14] which are discussed in the proceeding sections. By having different combinations of those switches will steer the main beam in different directions. Resonance frequency of the antenna is around 2.4 GHz at which the gain is about 5 dB. The details of antenna design and analysis are given in coming sections.

2. Antenna Design

First of all, a single patch antenna was designed for 2.4GHz and then it was combined with another patch to increase the degree of freedom. The front view of proposed antenna is given in Fig 1, which shows the complete geometry of the proposed antenna. For switches, PIN diodes BAR 64 from Infineon were used which are explained in Figures 2 and 3. Equivalent circuit of the PIN diode in ON state is shown in Fig 2 in which, parallel combination of resistor and inductor was connected in series with capacitor. Fig 3 shows the equivalent circuit for PIN diode in OFF state, which was the series combination of a resistor and capacitor [15]. PIN diodes were connected in between the feeding point and patches. The substrate used was FR-4 which has $\mathcal{E}_r = 4.3$.

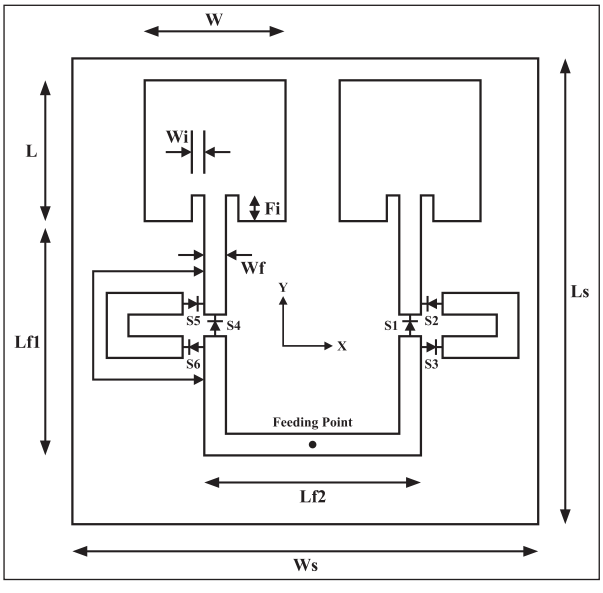

Fig 1. Front view of the proposed two element array

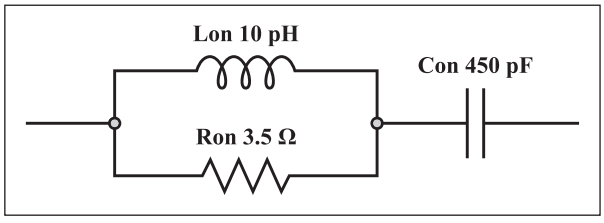

Fig 2. Representation of PIN diode in ON state

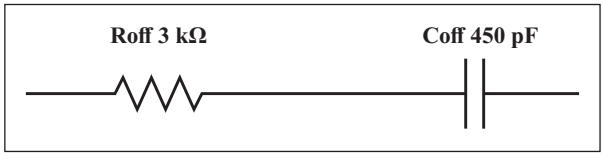

Fig 3. Representation of PIN diode in OFF state

Fig 4 shows the side view of the proposed antenna. A 50Ω coaxial cable was used to feed the antenna and a 100Ω microstrip transmission line was used to interconnect the two patches. Values of all parameters are given in Table 1. All these values were founded for operation at 2.4GHz. The transmission line width was adjusted such that it had a characteristic impedance of 100Ω. For this purpose, the famous formulas discussed in [16] was used for finding the transmission line width. Further, the transmission line was connected to that point in patch antenna at which almost 100Ω impedance matching was obtained. Therefore, the inset feed used as at the edges of the antenna impedance was not 100Ω.

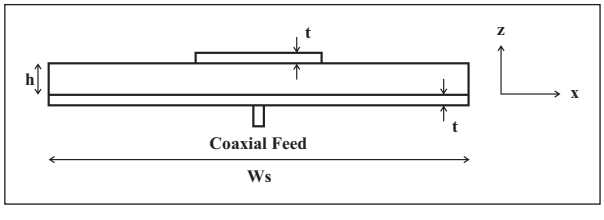

Fig 4. Side view of the proposed two element array

Table 1. Dimensions of proposed two element array

Antenna Dimensions	
Parameter	**Values**
Ls	200 mm
Ws	200 mm
L	27.75 mm
W	38.4 mm
h	3.2 mm
Wi	1.5 mm
Fi	10 mm
Lf1	97.44 mm
Lf2	59.93 mm
Ld	30.15 mm
Wf	1.45 mm
t	0.1 mm
Width of switch	2 mm

There were three different combinations of the switches as given below.

2.1 Condition-1

When S1 and S4 are ON and all other switches were OFF i.e. direct feeding. Both patches would receive the signal at the same time.

2.2 Condition-2

When S2, S3 and S4 were ON and all other switches were OFF i.e. right sided patch was fed with almost λ/2 delay line and left sided patch was fed directly.

2.3 Condition-3

When S1, S5 and S6 are ON and all other switches were OFF i.e. right sided patch was fed directly and left sided patch was fed with almost λ/2 delay line.

3. Results and Discussion

The proposed antenna was simulated and analysed in the Microwave Studio of Computer Simulation Technology (CST). The S-Parameter results are shown in Fig 5. This S-Parameter plot showed that in all three cases, the antenna was covering 2.4GHz band with good return loss. For condition-1, bandwidth of antenna was about 180MHz whereas for condition-2 and condition-3, the bandwidth was about 260MHz.

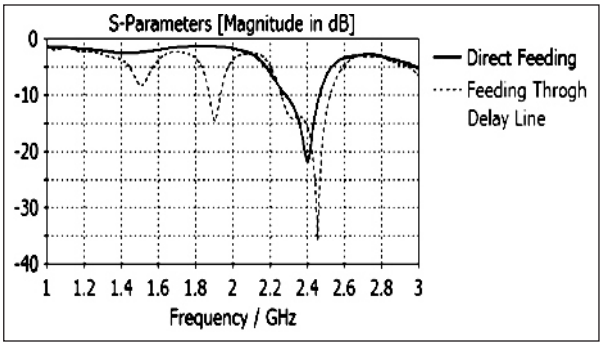

Fig 5. S-Parameter Plot for the proposed Antenna

Fig 6(a) and Fig 6(b) showed the plots for real and imaginary parts of Z- Matrix, respectively. These Figures showed that real part of impedance was approaching 50Ω and imaginary part as 0Ω at the resonance frequency and hence showed the impedance matching of antenna array with the 50Ω coaxial cable. 3D Radiation Patterns for Condition-1, Condtion-2 and Condtion-3 are shown in Fig 7, 8 and 9, respectively. Fig 7, 8 and 9 clearly showed that radiation pattern had changed significantly.

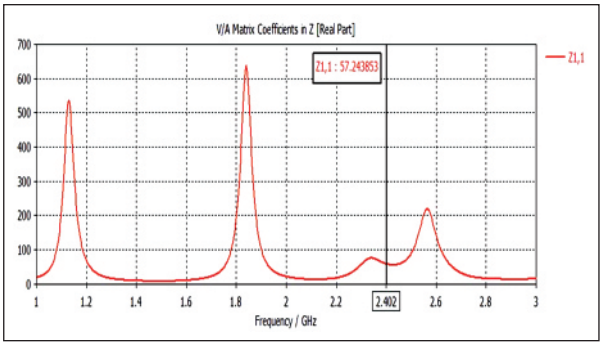

Fig 6(a). Real Part of Z-Matrix

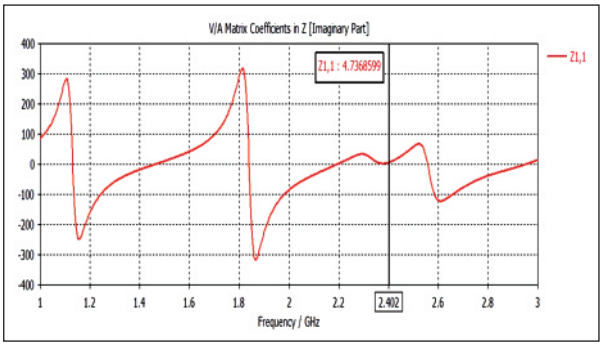

Fig 6(b). Imaginary Part of Z-Matrix

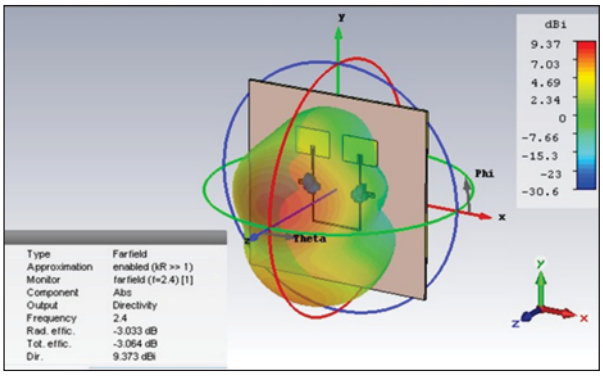

Fig 7. 3D Radiation Pattern Condition-1 (Direct Feeding)

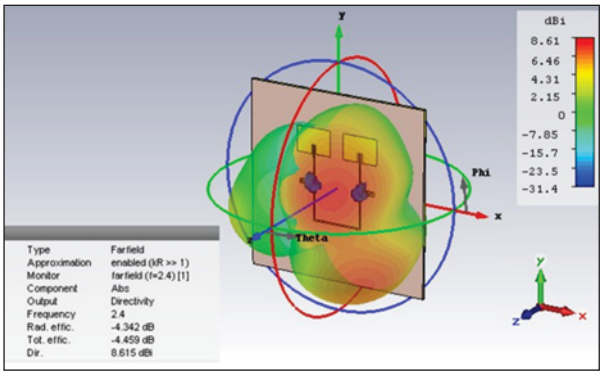

Fig 8. 3D Radiation Pattern Condition-2 (Right side patch fed with λ/2 delay line)

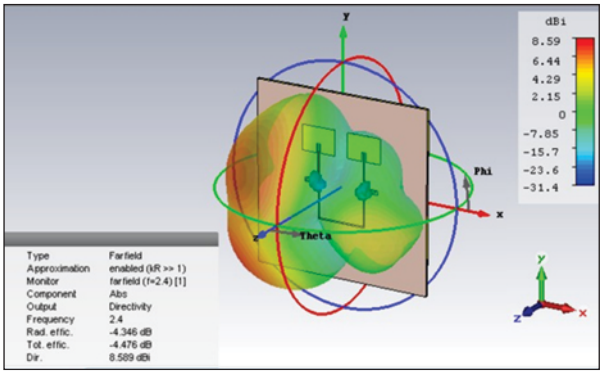

Fig 9. 3D Radiation Pattern Condition-3 (Left side patch fed with λ/2 delay line)

Fig 10, 11 and 12 portrayed another way of representing the concept of Fig 7, 8 and 9, respectively. Fig 10 showed that maximum radiation was at $\theta = 10°$, $\varphi = 85°$, Fig 11 showed the maximum radiation at $\theta = 30°$, $\varphi = 30°$, and Figure12 showed maximum radiation at $\theta = 30°$, $\varphi = 150°$. So radiation pattern has changed for different combination of switches.

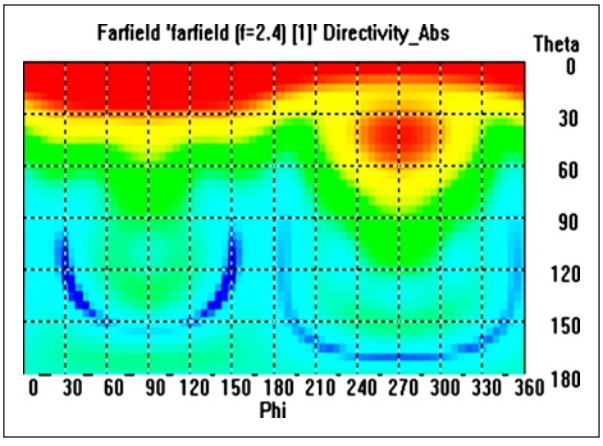

Fig 10. 2D Radiation Pattern Condition-1 (Direct Feeding) Maximum Directivity is at θ = 10°, φ = 85°

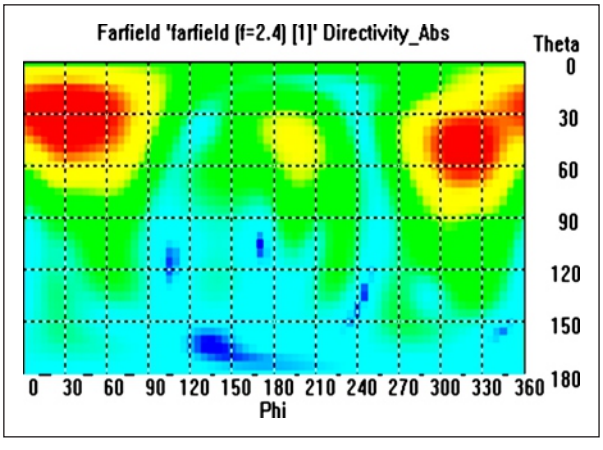

Fig 11. 2D Radiation Pattern Condition-2 (Right side patch fed with λ/2 delay line) Maximum Directivity is at θ = 30°, φ = 30°

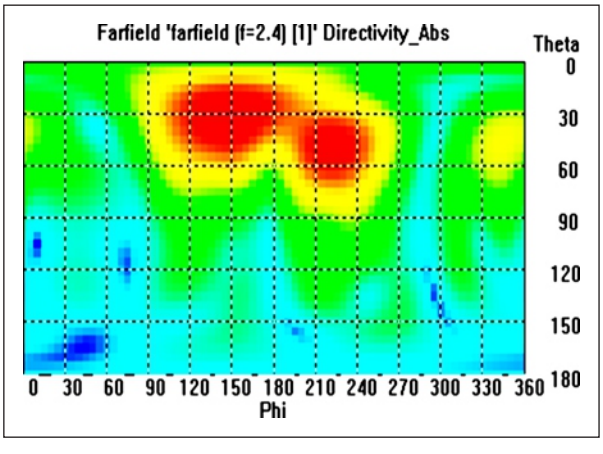

Fig 12. 2D Radiation Pattern Condition-3 (Left side patch fed with λ/2 delay line) Maximum Directivity is at θ = 30°, φ = 150°

Fig 13 showed the polar plot of radiation pattern for the stated three conditions. This polar plot was drawn by considering those planes for which directivity was maximum. Fig 14 showed the plot for maximum gain for the stated conditions. This plot showed that for the required frequency, the antenna exhibited improved properties. In order to further increase the gain, the number of patches were increased which would also give more degrees of freedom to steer the beam in different directions.

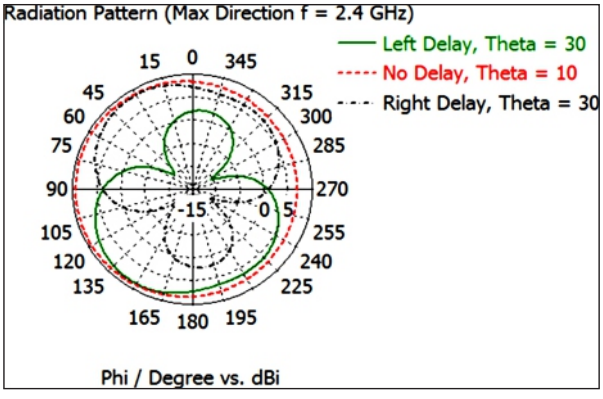

Fig 13. Maximum direction Radiation Pattern Plot for all of the three conditions i.e. θ = 10° cut for Condition-1, θ = 30° cut for Condition-2 and Condition-3

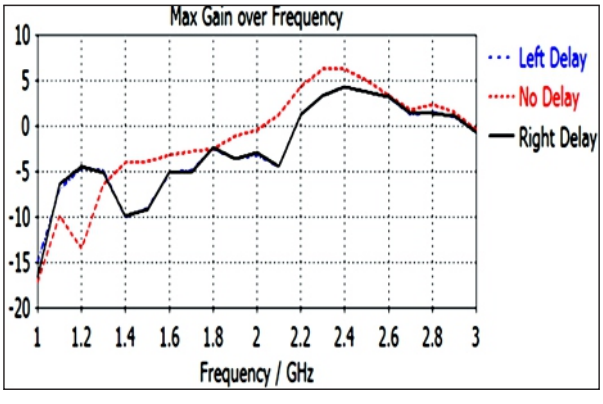

Fig 14. Maximum gain Vs. Frequency plot for the stated three conditions

Moreover, by changing the substrate the relative permittivity changed and hence it would change the frequency of operation, e.g. if we use Rogers RO3203 then resonance frequency changes to 2.868GHz as shown in Fig 15. To shift the resonance frequency back to 2.4GHz one has to change all antenna parameters.

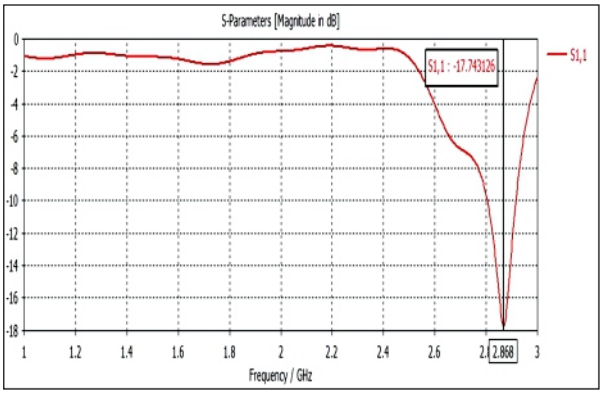

Fig 15. S-Parameters plot with Rogers RO3203

4. Conclusion

The results showed that by using feeding delay technique, the pattern reconfigurable antennas could be designed with less variation in other properties like S-Parameter, Directivity & Gain etc. Furthermore, pattern reconfigurable antennas increase the coverage area and the signal could be moved to the direction of maximum efficiency. PIN diodes were used for changing the main beam in desired direction. These PIN diodes are suitable and cost-effective for designing reconfigurable antennas as they provide fast switching and are easily fabricated on the Printed Circuit Board (PCB) with the antenna.

Acknowledgments

The authors wish to acknowledge the support provided for this research by the Department of Electrical Engineering, University of Engineering & Technology, Peshawar, KPK, Pakistan.

References

[1] Stutzman WL, Thiele GA. Antenna theory and design. John Wiley & Sons, 2012.

[2] Parashar, R., Bhomia, Y., Soni, D. and Saraswat, R.K. A Multi-Band Frequency Reconfigurable Antenna for Wireless Applications. IEEE International Conference on Computing, Communication and Networking Technologies (ICCCNT) (pp. 1-4), 2019.

[3] Altamirano, J.C., Rodríguez, D.N., Sarango, V.A., Tonato, G.H., Navarro-Méndez, D. and Molina, H.B. Frequency Reconfigurable Antenna Using Double Phase-Shifted Feed. IEEE Microwave Theory and Techniques in Wireless Communications (MTTW), Vol. 1, pp. 27-29, 2019.

[4] Ji LY, Qin PY, Guo YJ, Ding C, Fu G, Gong SX. A wideband polarization reconfigurable antenna with partially reflective surface. IEEE Transactions on Antennas and Propagation, vol. 64, no. 10, pp. 4534–4538, 2016.

[5] Lin W, Wong H. Multi-polarization reconfigurable circular patch antenna with l-shaped probes. IEEE Antennas and Wireless Propagation Letters, 2017.

[6] Shah, S.S., Bashir, S., Farooq, M. and Azeem, A. Radiation Pattern Reconfigurable Antenna Integrated With Electromagnetic Bandgap (EBG) Reflector. International Conference on Mathematics, Actuarial Science, Computer Science and Statistics (MACS) (pp. 1-5), 2019.

[7] Row JS, Tsai CW. Pattern reconfigurable antenna array with circular polarization. IEEE Transactions on Antennas and Propagation, vol. 64, no. 4, pp. 1525–1530, 2016.

[8] Deng Z, Guo X, Wei H, Gan J, Wang Y. Design, analysis, and verification of Ka-band pattern reconfigurable patch antenna using RF mems switches. Micromachines, vol. 7, no. 8, p. 144, 2016.

[9] Gopalakrishnan, J.B., Sabapathy, T., Jusoh, M., Al-Bawri, S., Yaasin, M.N., Osman, M.N., Rahim, H.A., Mat, M.H., Majid, H.A., Ali, T. and Wahab, Y.A. Radiation Pattern Reconfigurable FM Antenna. In Journal of Physics: Conference Series, Vol. 1339, No. 1, 2019.

[10] Aris M, Ali M, Rahman NA, Pasya I, Fauzi N. Simulation of radiation pattern reconfigurable microstrip patch antenna using feeding delay line technique. In the proceedings of IEEE Asia-Pacific Conference on Applied Electromagnetics, pp. 305–309, 2016.

[11] Yan S, Vandenbosch GA. Wearable pattern reconfigurable patch antenna. In the proceedings of IEEE International Symposium on Antennas and Propagation pp. 1665–1666, 2016.

[12] Cleetus RMC, Sudha T. Design and analysis of a frequency and pattern reconfigurable microstrip patch antenna for wireless applications. In the proceedings of IEEE International Conference on Control Communication and Computing (ICCC), pp. 287–291, 2013.

[13] Tilanthe P, Sharma P. A pattern reconfigurable patch antenna with square ring shaped parasite radiator. In the proceedings of IEEE International Conference on Applied Electromagnetics (AEMC), pp. 1–4, 2009.

[14] Purisima MCL, Salvador M, Agustin SGP, Cunanan MT. Frequency and pattern reconfigurable antennas for community cellular applications. In the proceedings of IEEE Region 10 Conference (TENCON), pp. 3767–3770, 2016.

[15] Ismail M, Rahim M, Majid H. The investigation of pin diode switch on reconfigurable antenna. In the proceedings of IEEE International Conference on RF and Microwave (RFM), pp. 234–237, 2011.

[16] Pozar DM. Microwave engineering. John wiley & sons, 2009.

ISSN NO. 2706-9648

Pakistan Journal of Engineering

For online access, please visit:
journal.pec.org.pk

FEATURE EXTRACTION AND CLASSIFICATION OF SURFACE EMG SIGNAL OF RIGHT ARM TO MAKE AN ARTIFICIAL HAND AS ASSISTIVE DEVICE FOR UPPER LIMB AMPUTEES

Osama Saeed, Bilal Fattah, Jahanzaib Ali, Faiza Niazi, Sarmad Shams, Ali Asghar Ali, Mubsir Bin Saeed

ARTICLE INFO

Article History:

Accepted 16 Oct 2020

Published on 25 Oct 2020

Keywords

Artificial Hand, EMG Classification, Feature Extraction, Prosthesis, Neural Network, Assistive device, Prosthetic hand, Robotic hand, EMG, Signal processing

ABSTRACT

The crucial technique of this era for electromyography (EMG) signal classification is the Artificial Neural Network which is the mimic of human neural network. The human machine interface has been done by this artificial network to integrate artificial hand and the human arm. The complexity of the design of artificial hand, the complex computation of model of neural network, the high cost of design and computation resist the implementation of artificial hand. This study has reduces the complexity of design by selecting the simple open source design of open bionics "Ada Hand (V1.1)". The structure of this mechanical design has the string mechanism which makes its assembling easy enough and the material of ninja-flex and Poly-lactic acid (PLA) used for its 3D printing reduces the manufacturing cost of the artificial hand. The programming of the algorithm has been done by using the neural network classifier for the learning of artificial hand that which movement belongs to which class. The flexor and extensor muscles of right arm have been used to acquire the surface electromyography (sEMG) signal with the help of metal electrodes of Gravity Analog EMG Sensor. These two channel data acquisition from extensor digitorum communis (EDC) and the flexor digitorum superficialis (FDS) muscles have been filtered and amplified by the integrated circuit of Gravity Analog EMG sensor. Wavelength is the first extracted feature which results a vector of the same length of the original data. From this resulted vector of wavelength, other features like root mean square (rms), standard deviation (std), variance (var) and mean absolute deviation (mad) have been extracted. By using these features, the neural network classifier classifies

three classes which are wrist extension, fist and wrist flexion. When the user performs extension movement, the artificial hand will classify it as class one and perform index movement. Similarly, when the user performs fist movement, the artificial hand will classify it as class two and perform fist movement too. And when the user performs flexion movement, the artificial hand will classify it as class three and perform pinch movement. The softmax and sigmoid function of neural network classifier also contributed to perform the multiclass classification. The sEMG data was acquired from seven different subjects in which four were men and three were women. Both groups were asked to perform three movements i.e. extension, fist and flexion in three different positions i.e. lying, standing and sitting. The overall accuracy of the algorithm is up to 95% which is enough to use this artificial hand in the application of assistive device for the upper limb amputees and make their life independent.

1. Introduction

The world population is about 6.7 billion in which about 10 million are amputees, having 3 million the amputees of arm and 0.1 million hand/wrist amputees [1]. They cannot perform their daily routine work such as drinking, eating, opening door, dialing phone number and typing, picking up keys, cards or small objects. They can't shake their hands, they can't interact with people cheerfully, and they need assistance for doing their routine work. In short, they are totally dependent on others.

Electromyography (EMG) based Artificial Hands are assisting them for their daily routine work. Different gestures of hand give different pattern of signals. By using these signals, the movement of artificial hand could be accomplished Fig 1 EMG is the study of muscle's action potential. The EMG signal gives raw data which has to become in understandable form. For this purpose, some signal processing techniques are used.

Best signal processing methods such as recognition of signal pattern [10] have shown the ability to control different DOFs. Various research studies have recognized the pattern of EMG for controlling Artificial Hand which give maximum classification accuracies by using the techniques of Pre-processing and then extraction of signal features and classification [10, 11, and 12].

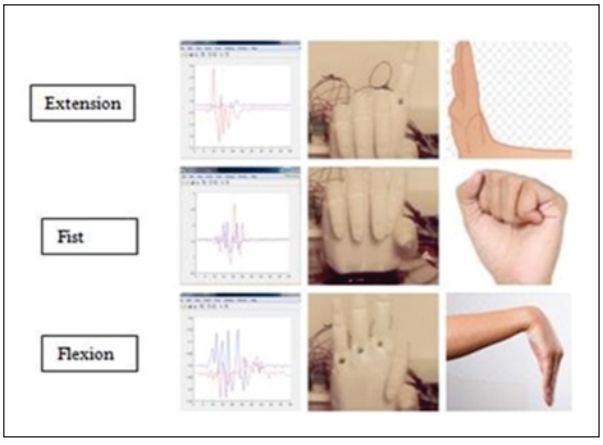

Fig 1. Column 1 shows graph of gestures of column 3 human hand and column 2 is the response of Artificial Hand

EMG signals have been acquired by attaching the electrodes of EMG sensors on the forearm of subject. Better control over artificial hand needs many EMG sensors, raising essentially the expense and system complexity. According to researches, placement of four [2, 3], six [4, 5], eight [6] and ten [7] bipolar electrodes were placed on the forearm. Single channel (sEMG) investigation is favored over multi-channel because of amputee's comfort and less expense. The single EMG channel already contributed two gestures of extension and flexion [8, 9]. This paper presents a simplest approach to achieve three gestures (fist, extension and flexion)

by using two EMG channels. The use of two sensors reduces the cost of components; gives comfort to the user and make the design simple. The aim of this paper was to make a feature vector which enabled the Artificial Hand to perform different gestures to assist the amputees in their daily routine.

The modern prosthetic hands can do many functions but have a high price as unaffordable and not everyone can buy it. In 2012, Hanger Prosthetics is specialized in custom artificial and orthotic devices; a well-known in the robotics community and industry. They introduced the cost of the hand would be a staggering $60,000. In 2012, Michelangelo Hand has the most developed artificial hand in the market. But unfortunately the hand cost is $100,000. There is another prosthetic hand which has low cost comparing to above mentioned prosthetic hands but it is just a mechanical design which have an opposable thumb. The computer program and algorithms are not installed in it and bearing the cost around $3,000 [19]. Effort has been made in this study to decrease the price of manufacturing and make it affordable for every amputee by using the ninja-flex and PLA material to make an open source prosthetic hand design of Open Bionics of version (Ada V1.1) as shown in Fig 2.

Fig 2. Open source design of Ada hand. V1.1
https://openbionicslabs.com/obtutorials/ada-v1-assembly

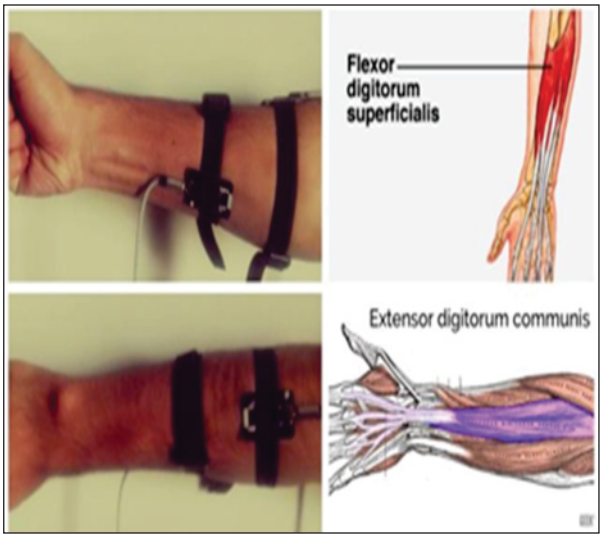

Fig 3. Placement of sensors at EDC and FDS muscles

2. Methodology

To robust the application of Artificial Hand and simplifying the system of EMG-signal pattern recognition, a simple extraction of feature vector is introduced here which is based on time domain. These features were classified by the artificial neural network classifier of supervised machine learning.

2.1 Data Collection

For the collection of data, the procedure of surface Electromyography (sEMG) was performed on seven healthy subjects in which four were male subjects and three were female subjects at the age of 20-25 by placing two sEMG sensors at the forearm. The electrodes were place at extensor digitorum communis (EDC) and flexor digitorum superficialis (FDS) muscles as shown in Fig 3. Both the muscles extend the medial four fingers of the hand and are responsible for the extension and flexion of hand. For the comfort of subject and the durability of sensors, the dry electrode was used instead of gel electrodes. This reduced the cost of buying gel electrodes every time because gel electrodes are disposables and can be used just one time.

2.2 Observations

The sensor was placed at the right forearm of subjects at the EDC and FDS muscles. The subjects were asked to perform wrist extension, fist and wrist flexion movement of right hand in three different session lying, sitting and standing. All the subjects did the mentioned three movements for the duration of four second to record the pattern of these three movements. By following this method, the data was observed. Usually the EMG data is in raw data form which has to be in understandable form to recognize the pattern of different gestures. For pattern recognition of EMG signal, the following signal processing steps were used:

- Preprocessing
- Feature extraction
- Classification

2.3 Preprocessing

The EMG signal is in the form of raw data which have unwanted signal which has to be filtered; noise which has to be removed; and the signal is also very weak which has to be amplified. Preprocessing the signal means removal of noise, filtering and amplifying the signal. We used the Gravity Analog EMG sensor which attached noise removing and signal strengthening circuit. The sensor maximize sEMG signal and reduces noises by input of differential and circuit of analog filter [27]. The data was acquired at the default sampling rate of approximately 100Hz by using "readVoltage" command of matlab software [28]. This sensor produced the filtered, amplified and noise free signal which required some more signal processing in which its features were to be extracted.

2.4 Feature Extraction

Feature extraction is the technique to acquired hidden information from signals by applying formulae. Many researchers showed that various features sets help to acquire the useful information from EMG data for the application of making algorithms to control Artificial Hand. The feature is set of four features: waveform length (WL), zero crossings (ZC), mean absolute value (MAV), and slope sign changes (SSC) which were used to make algorithm as invariant to upper limb movement for the classification of EMG signal [17]. Another feature is extracting method which extracts a power spectrum feature set from the domain of time [18]. A new feature set was therefore introduced to make an algorithm for controlling three movements of Artificial Hand i.e. root mean square (rms), standard deviation (std), variance (var), mean absolute deviation (mad) and waveform length (WL).

Wavelength refers to the length or distance between two neighboring points of signal.

$$WL = \sum_{i=1}^{N} |x_i - x_{i-1}| \quad \text{Eq. 1}$$

Variance measures how far a set of numbers are spread out from their average value.

$$Variance = \frac{(x-\mu)^2}{N} \quad \text{Eq. 2}$$

Standard deviance measure how close and far is the values from its mean.

$$SD = \sqrt{\frac{\sum (r_i - r_{avg})^2}{N-1}} \quad \text{Eq. 3}$$

Mean absolute deviation are the average absolute deviation about any certain point of a data set

$$MAD = \frac{\sum_{i=1}^{N} |x_i - \bar{x}|}{N} \quad \text{Eq. 4}$$

Root mean square are the square root of mean square.

$$RMS = \sqrt{\frac{\sum_{i=1}^{N} x_i^2}{N}} \quad \text{Eq. 5}$$

2.5 Classification

After the extraction of features and making feature set, it was required to choose which classifier was good for the algorithm. The EMG signal processing uses different algorithms to control the Artificial Hand by classifying the different set of feature values results in different hand gestures. Some classifiers give better performance than others depending on the specific application they are used. Other scientists suggest to use the classifier of Fuzzy logic [20,21], which gives input of subject's data in the algorithm, and recognizes itself the patterns of EMG. The fuzzy logic classifiers show poor performance with small data sets of training [22]. Neural Network classifiers are broadly utilized [23,24] due to better performance in simple and complex cases. The network of neuron is broadly used as the Classification model. The development of the network of neuron has a remarkable background and a wide range of achievements in works of scientists. The recent growth has a lot of interest for Classification. The implementation of classification algorithms has various forms such as linear discriminant analysis (LDA) and Support Vector Machine (SVM). The network of neuron is one of them.

This paper utilizes the technique of multilayer neural network to make a model which contains a single hidden layer (Fig 4). There were set 5 input nodes; and three classes for classification, so that the network had 3 outputs. The function of softmax acts as the function of activation for the nodes of output. The function of sigmoid was utilized for the function of activation of hidden layers. In 1986, the invention of the algorithm of back-propagation resolved the problem of training for the multi-layer network of neuron [25]. The algorithm of back-propagation has importance for developing a method of system to find the hidden layer errors. After finding the errors hidden layer, the learning rule of Stochastic Gradient Descent (SGD) adjusted the weights of network.

The algorithm of MultiClass classification used the rule of learning for multiclass classification by utilizing the SGD and back propogation techniques. It acquired the input in the form of weights and datasets of training and gave the output in the form of trained weights. The logarithm definition says that the output should be within the range of 0-1. That's why, the Stochastic Gradient Descent (SGD) apply activation functions of sigmoid and softmax.

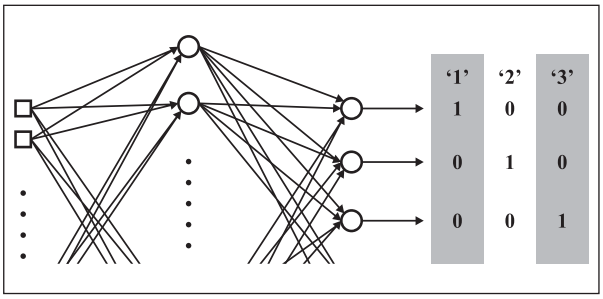

Fig 4. Multilayer Neural Network

The activation function sigmoid was used only for the input weights and not for output layer. The softmax activation function was used for both input weights, and for the inputs to the other output nodes.

SIGMOID

$$y = 1 / (1 + \exp(-x)) \text{ SOFTMAX} \qquad \text{Eq. 6}$$

SOFTMAX

$$y = \exp(x) / \text{sum}(\exp(x)) \qquad \text{Eq. 7}$$

3. Results

The performance of seven subjects at three different sessions (lying, sitting and standing) in all cases gave accuracy up to 95%. The result of session one in which subject was asked to lie-down and performed the three gestures (fist, extension and flexion) gave the average of 98.37% as shown in Fig 5. In session two, the subject was asked to stand up and performs the three gestures (fist, extension and flexion) which produced the accuracy of 100% (Fig 6). The last session gave the approximate percentage of accuracy 97.73% (Fig 7), in which subject was asked to sit-down and performed the three gestures (fist, extension and flexion).

	EX	FI	FL
EX	97.1 %	1.4 %	1.5 %
FI	0 %	100 %	0 %
FL	1.1 %	0.9 %	98 %

Fig 5. The results of session 1 when subject was lying

	EX	FI	FL
EX	100 %	0 %	0 %
FI	0 %	100 %	0 %
FL	0 %	0 %	100 %

Fig 6. The results of session 2 when subject was standing

	EX	FI	FL
EX	99.1 %	0.8 %	0.1 %
FI	1.6 %	98.1 %	0.3 %
FL	2.4 %	1.6 %	96 %

Fig 7. The results of session 3 when the subject was sitting

4. Discussion

The amputees who would use the presented Artificial Hand has to be trained by performing the gestures at different positions and understanding the force they should give to this hand and the knowledge of placement of EMG electrodes. This work is good for the specific application of amputees, to make it enable for the general use as one requires a high data sets of healthy and amputees. Another classifier would also increase the functionality and classes of the artificial hand.

5. Conclusions

This paper introduced a Neural Network based model in which the EMG sensor of two channels was used to classify three daily movements to make a robust Artificial Hand. The results showed the performance of Gravity Analog EMG sensor as it acquired the signal as well as the preprocessing of signal. The root mean square (rms), standard deviation (std), variance (var), mean absolute deviation (mad) and waveform length (WL) were used as features for classifier. These features were enough for Neural Network classifier to classify the signal which reduced the number of computations performed. The stochastic gradient descent (SGD) learning rule was used by classifier for the learning of Artificial Hand. The softmax and sigmoid was also used as activation functions for the network. The future work is to use various EMG sensors and feature sets for making more classes. Some other classifiers should also be used for making more dexterous model. This hand can perform some movements of daily routine such as holding cup and glass, hand shake, opening door, dialing phone number and typing, pick up key, cards or small objects.

References

[1] Maurice LeBlanc, MSME, CP "Give Hope - Give a Hand" - The LN-4 Prosthetic Hand, 2008.

[2] G.R. Naik, D.K. Kumar, et al., Twin svm for gesture classification using the surface electromyogram, IEEE Trans.Inf. Technol. Biomed. 14 (2) (2010) 301–308.

[3] A.B. Ajiboye, et al., A heuristic fuzzy logic approach to emg pattern recognition for multifunctional prosthesis control, IEEE Trans. Neural Syst. Rehabil. Eng. 13 (3) (2005) 280– 291.

[4] D. Yang, J. Zhao, Y. Gu, L. Jiang, H. Liu, Emg pattern recognition and grasping force estimation: improvement to the myocontrol of multi-dof prosthetic hands, in: IEEE/RSJ International Conference on Intelligent Robots and Systems. IROS 2009, IEEE, 2009, pp. 516–521.

[5] A.H. Al-Timemy, G. Bugmann, J. Escudero, N. Outram, Classification of finger movements for the dexterous hand prosthesis control with surface electromyography, IEEE J. Biomed. Health Inform. 17 (3) (2013) 608–618.

[6] C. Cipriani, C. Antfolk, M. Controzzi, G. Lundborg, B. Rosén, M.C. Carrozza, F. Sebelius, Online myoelectric control of a dexterous hand prosthesis by transradial amputees, IEEE Trans. Neural Syst. Rehabil. Eng. 19 (3) (2011) 260–270.

[7] V.D.S.P.S. Bitzer, Learning emg control of a robotic hand: towards active prostheses, in: Proceedings 2006 IEEE International Conference on Robotics and Automation, ICRA 2006, IEEE, 2006, pp. 2819–2823.

[8] T. Peters, An assessment of single-channel emg sensing for gestural input, in: Dartmouth Computer Science Technical Report, 2015/767, 2014, pp. 1–14.

[9] S. Mane, R. Kambli, F. Kazi, N. Singh, Hand motion recognition from single channel surface emg using wavelet & artificial neural network, Procedia Comput. Sci. 49 (2015) 58–65.

[10] E Scheme, K. Englehart, Electromyogram pattern recognition for control of powered upper-limb prostheses: state of the art and challenges for clinical use, J. Rehab. Res. Dev. 48 (2011) 643.

[11] Y. Geng, P. Zhou, G. Li, Toward attenuating the impact of arm positions on electromyography pattern-recognition based motion classification in transradial amputees, J. Neuroeng. Rehabil. 9 (2012) 74.

[12] A.M. Simon, L.J. Hargrove, B.A. Lock, T.A. Kuiken, A decision-based velocity ramp for minimizing the effect of misclassifications during real-time pattern recognition control, IEEE Trans. Biomed. Eng. 58 (2011) 2360–2368.

[13] E. Scheme, A. Fougner, Ø. Stavdahl, A.D.C. Chan, K. Englehart, Examining the adverse effects of limb position on pattern recognition based myoelectric control, Anonymous 2010 annual international conference of the IEEE engineering in medicine and biology (2010) 6337–6340.

[14] Fougner, E. Scheme, A.D. Chan, K. Englehart, Stavdahl, Resolving the limb position effect in myoelectric pattern recognition, IEEE Trans. Neural Syst. Rehabil. Eng. 19 (2011) 644–651. AnandKumarMukhopadhyayaSumanSamuib

[15] An experimental study on upper limb position invariant EMG signal classification based on deep neural network, Biomedical Signal Processing and Control, Volume 55, January 2020, 101669.

[16] Diego Ferigoa, A Case Study of a Force-myography Controlled Bionic Hand Mitigating Limb Position Effect, Journal of Bionic Engineering, Volume 14, Issue 4, October 2017, Pages 692-705.

[17] Mads Jochumsena,Asim Warisa,Ernest Nlandu Kamavuakoc, The effect of arm position on classification of hand gestures with intramuscular EMG, Biomedical Signal Processing and Control, Volume 43, May 2018, 1-8.

[18] Rami N. Khushaba,Maen Takruri,Jaime Valls Miroa,Sarath Kodagoda,Towards limb position invariant myoelectric pattern recognition using time-dependent spectral features, Neural Networks Volume 55, July 2014, 42-58.

[19] Paul Ventimiglia, Design of a Human Hand Prosthesis, 2012.

[20] F.H.Y. Chan, Y.-S. Yang, F.K. Lam, Y.-T. Zhang, P.A. Parker, Fuzzy emg classification for prosthesis control, IEEE Trans. Rehabil. Eng. 8 (3) (2000) 305–311.

[21] L.-X. Wang, Adaptive fuzzy systems and control: design and stability analysis,IEEE Trans. Fuzzy Syst. 1 (2) (1993) 146– 155.

[22] S. Godil, M. Shamim, S. Enam, U. Qidwai, Fuzzy logic: A "simple" solution for complexities in neurosciences? Surgical Neurology International 2 (2011) 24.

[23] Soares, A. Andrade, E. Lamounier, R. Carrijo, The development of a virtual myoelectric prosthesis controlled by an emg pattern recognition system based on neural networks, J. Intell. Inf. Syst. 21 (2) (2003) 127–141.

[24] X. Zhang, X. Chen, W.-h. Wang, J.-h. Yang, V. Lantz, K.-q. Wang, Hand gesture recognition and virtual game control based on 3d accelerometer and emg sensors, Proceedings of the 14th International Conference on Intelligent User Interfaces, ACM (2009) 401–406.

[25] Phil Kim, MATLAB Deep Learning With Machine Learning, Neural Networks and Artificial Intelligence.

[26] Mahmoud Tavakoli, Carlo Benussi, Pedro Alhais Lopes, Luis Bica Osorio, Anibal T. de Almeida, Robust hand gesture recognition with a double channel surface EMG wearable armband and SVM classifier, Biomedical Signal Processing and Control 46 (2018) 121-130.

[27] Gravity: Analog EMG Sensor by OYMotion, doi: https://www.dfrobot.com/product-1661.html.

[28] Default sampling rate of analog data acquire in matlab, doi: https://it.mathworks.com/matlabcentral/answers/327998-maximum-sampling-frequency-of-analog-input-through-arduino-uno#answer_354308.

Pakistan Journal of Engineering

PAKISTAN ENGINEERING COUNCIL
Ataturk Avenue (East), G-5/2, P.O. Box: 1296, Islamabad - Pakistan.
Ph: (+92 51) 287 6702, 920 6974, 921 9500
Website: https://www.journal.pec.org.pk